Article

Not peer-reviewed version

Insight into Romanian Wild-Grown *Heracleum sphondylium*: Development of a New Phytocarrier Based on Silver Nanoparticles with Antioxidant, Antimicrobial and Cytotoxicity Potential

Adina-Elena Segneanu , Gabriela Vlase , Titus Vlase , Ludovic Everard Bejenaru * , George Dan Mogoșanu , Gabriela Buema , Maria Viorica Ciocîlteu , Cornelia Bejenaru

Posted Date: 27 August 2024

doi: 10.20944/preprints202408.1706.v1

Keywords: *Heracleum sphondylium*; silver nanoparticles; phytocomplex; secondary metabolites; antioxidant potential; antimicrobial screening; *in vitro* cytotoxicity

Article

Insight into Romanian Wild-Grown *Heracleum sphondylium*: Development of a New Phytocarrier Based on Silver Nanoparticles with Antioxidant, Antimicrobial and Cytotoxicity Potential

Adina-Elena Segneanu [1], Gabriela Vlase [1,2], Titus Vlase [1,2], Ludovic Everard Bejenaru [3,*], George Dan Mogoşanu [3], Gabriela Buema [4], Maria Viorica Ciocîlteu [5] and Cornelia Bejenaru [6]

[1] Institute for Advanced Environmental Research, West University of Timişoara (ICAM–WUT), 4 Oituz Street, 300086 Timişoara, Timiş County, Romania
[2] Research Center for Thermal Analyzes in Environmental Problems, West University of Timişoara, 16 Johann Heinrich Pestalozzi Street, 300115 Timişoara, Timiş County, Romania
[3] Department of Pharmacognosy & Phytotherapy, Faculty of Pharmacy, University of Medicine and Pharmacy of Craiova, 2 Petru Rareş Street, 200349 Craiova, Dolj County, Romania
[4] National Institute of Research and Development for Technical Physics, 47 Dimitrie Mangeron Avenue, 700050 Iaşi, Iaşi County, Romania
[5] Department of Analytical Chemistry, Faculty of Pharmacy, University of Medicine and Pharmacy of Craiova, 2 Petru Rareş Street, 200349 Craiova, Dolj County, Romania
[6] Department of Pharmaceutical Botany, Faculty of Pharmacy, University of Medicine and Pharmacy of Craiova, 2 Petru Rareş Street, 200349 Craiova, Dolj County, Romania
* Correspondence: ludovic.bejenaru@umfcv.ro

Abstract: Background: *Heracleum sphondylium*, a medicinal plant used in Romanian ethnopharmacology, proved to have a remarkable biological activity. The escalating concerns surrounding antimicrobial resistance led to a special attention to new efficient antimicrobial agents based on medicinal plants and nanotechnology. We report the preparation of a novel, simple phytocarrier that harnesses the bioactive properties of *H. sphondylium* and silver nanoparticles (HS-Ag system). Methods: The *H. sphondylium* low-metabolic profile was determined through gas chromatography–mass spectrometry and electrospray ionization–quadrupole time-of-flight–mass spectrometry. The morphostructural properties of the innovative phytocarrier were analyzed by X-ray diffraction, Fourier-transform infrared spectroscopy, Raman spectroscopy, dynamic light scattering, scanning electron microscopy, and energy-dispersive X-ray spectroscopy. The antioxidant activity was evaluated using total phenolic content, ferric reducing antioxidant power, and 2,2-diphenyl-1-picrylhydrazyl (DPPH) *in vitro* assays. The antimicrobial activity screening against *Staphylococcus aureus*, *Bacillus subtilis*, *Pseudomonas aeruginosa*, and *Escherichia coli* was conducted using the agar well diffusion method. 3-(4,5-Dimethylthiazol-2-yl)-2,5-diphenyltetrazolium bromide (MTT) assay estimated the *in vitro* potential cytotoxicity on normal human dermal fibroblasts (NHDF) and cervical cancer (HeLa) cells. Results: A total of 88 biomolecules were detected, such as terpenoids, flavonoids, phenolic acids, coumarins, phenylpropanoids, iridoids, amino acids, phytosterols, fatty acids. HS-Ag phytocarrier heightened efficacy in suppressing the growth of all tested bacterial strains compared to *H. sphondylium* and exhibited a significant inhibition of HeLa cell viability. Conclusions: The new HS-Ag phytocarrier system holds promise for a wide range of medical applications. The data confirms the capacity to augment pertinent theoretical understanding in the innovative field of antimicrobial agents.

Keywords: *Heracleum sphondylium*; silver nanoparticles; phytocomplex; secondary metabolites; antioxidant potential; antimicrobial screening; *in vitro* cytotoxicity

1. Introduction

 doi:10.20944/preprints202408.1706.v1

Heracleum sphondylium (*Apiaceae* family), commonly known as hogweed or cow parsnip, is widespread in Europe, parts of Asia, and northern Africa, and is present throughout Europe except for the extreme north and some Mediterranean regions [1–5]. In Romania, *H. sphondylium*, known locally as *brânca ursului*, is common nationwide in various forms, frequent from lowlands to mountainous regions, in thickets, hayfields, meadows, riparian zones, sparse forests, and rocky grasslands [4,6,7]. The species exhibits high variability, leading to many mentioned subspecies (nine in European flora, three in Romanian flora) [4–7].

H. sphondylium is a biennial or perennial species with a thick, branched rhizome. The aerial stem is well-developed, reaching heights of up to (150–) 200 (–350) cm and a 4–20 mm diameter. The leaves are highly variable, ranging from simple, undivided, or merely lobed to pinnatisect leaves with 3–5(7) asymmetrical, diversely lobed segments; the axil of the stem leaves is slightly swollen, rough-pubescent, or glabrous. The inflorescences are large, with umbels up to 25 cm in diameter, having up to 40 unequal rays, and with few or without bracts. The flowers have variously colored petals (white, yellow, pink, purple, greenish, or blue) and are often slightly pubescent externally. The ovary is glabrous, pubescent, or hispid. The fruits are strongly flattened, ellipsoidal, obovate, or nearly round, emarginate, with winged lateral ribs forming a delineated margin around them. The plants bloom from June to September [4–7].

H. sphondylium is used as a nutritional source in many regions globally; the stems, leaves, and inflorescences are utilized to obtain numerous preparations: e.g., in Eastern Europe and Northeastern Asia, various soups are made using this plant [1,2].

H. sphondylium roots, stems, leaves, and inflorescences are employed in traditional medicine in countries where it grows spontaneously to treat digestive disorders such as flatulence, dyspepsia, diarrhea, and dysentery, as well as hypertension, epilepsy, menstrual problems, and for wound healing, due to its analgesic, sedative, anti-infective, antioxidant, anticonvulsant, vasorelaxant, antihypertensive, carminative, tonic, and aphrodisiac properties [8–14].

Recent studies addressing the chemical composition of *H. sphondylium* have demonstrated the presence of a complex mixture of furocoumarins (bergapten, isopimpinellin, heraclenin), essential oil, polyphenolic compounds, phytosterols, pentacyclic triterpenes, and fatty acids [1–3,14–17]. Numerous research reported their multiple therapeutic properties, such as antioxidant, vasorelaxant, antimicrobial, antiviral, anti-inflammatory, antidiabetic, neuroprotective, and antitumor [1,12–14]. Despite its great pharmacological potential, most research focuses on several phytochemical categories extracted from different parts of this plant [1,12–14]. In addition, there is limited research on Romanian wild-grown *H. sphondylium* addressing only essential oil and phenolic compounds [8,16].

Furthermore, the variations of secondary metabolites amount to a function of various abiotic and biotic factors, growth stage, and extraction technique parameters (temperature, solvent polarity, duration, pH, etc.) dictate the herb's chemical profile and biological activity [18–22]. Conversely, recent research on natural compounds reported that several molecules exhibit low bioavailability due to reduced chemical stability and limited adsorption [23–25].

Antimicrobial resistance and tolerance emerge as paramount health concerns with severe repercussions on the therapeutic strategy of infectious diseases [24]. Antibiotic abuse or misuse for human health and the agri-food sector contributed significantly to rendering existing antimicrobials ineffective and exacerbating antimicrobial resistance. Without urgent measures, the depletion of antimicrobial alternatives will lead to a rise in infections related to antibiotic-resistant pathogens. It is urgent to identify new targeted antimicrobial agents against pathogenic microorganisms while mitigating the progression of antimicrobial resistance. Consequently, various strategies to overcome these challenges have been developed [25–27].

On the other hand, the implementation of nanotechnology in the biomedical field led to the development of advanced materials based on numerous phytoconstituents with high antimicrobial, antiviral, neuroprotective, and antitumor activity, which allowed not only overcoming these constraints but also a significant improvement of the pharmacological activity, controlled release, and specificity while minimizing toxicity [24–28].

 doi:10.20944/preprints202408.1706.v1

To this end, various nanoparticles (NPs), such as platinum, silver, gold, iron oxide, titanium dioxide, zinc, silica, and copper, have been reviewed for biomedical applications [29]. Among these, the silver nanoparticles (AgNPs) stood out due to their broad applicative potential from bioengineering to diagnosis, detection, gene and drug delivery, vaccines, and antimicrobial agents to wound and bone treatment [29–31]. Their extensive growth development is due to their outstanding size-related physicochemical (size, shape, surface plasmon resonance, surface charge, high surface-to-volume ratio, chemical stability, low reactivity) and biological (antimicrobial) properties [30,31]. In addition, AgNPs display uniquely tailored hydrophilic–hydrophobic balance through simple functionalization with various molecules, and the capability to cross the blood–brain barrier ensures the opening of new possibilities in the design of drug delivery systems and new performant antimicrobial agents [30–32]. In that sense, research on developing engineered herbal formulation assembles using NPs represents a significant advancement in enhancing the biological properties of phytoconstituents and enabling specific targeting and localization on surfaces [29].

This study investigates the preparation of a new phytocarrier through *H. sphondylium* loading with AgNPs (HS-Ag system) encompassing the physical and chemical characteristics and *in vitro* evaluation of antioxidant, antimicrobial, and cytotoxicity potential. To the best of our knowledge, the low-metabolite profile of *H. sphondylium* grown wild in Romania is reported for the first time in this study.

2. Results

2.1. GC–MS Analysis of H. sphondylium Sample

The compounds separated using gas chromatography–mass spectrometry (GC–MS) are depicted in Figure 1 and detailed in Table 1.

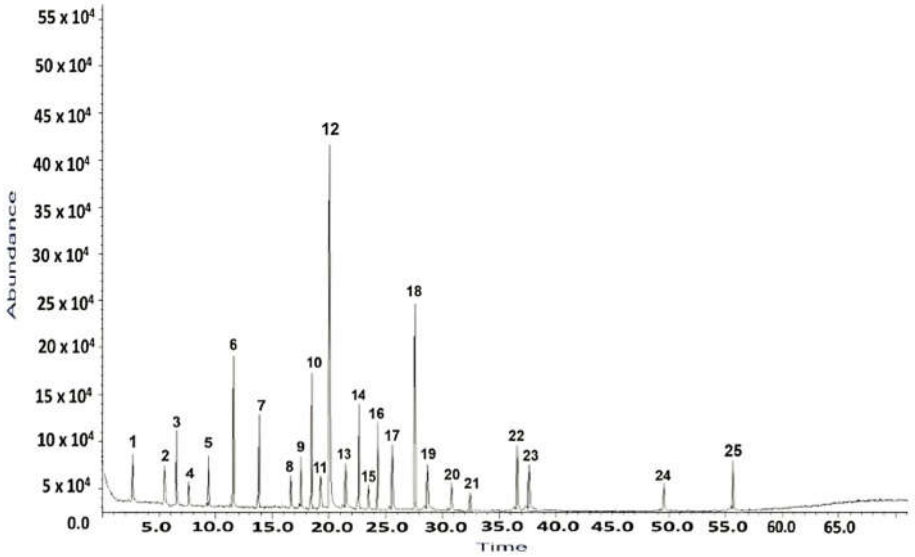

Figure 1. Total ion chromatogram of *H. sphondylium* sample.

Table 1. Main phytochemicals identified by GC–MS analysis of *H. sphondylium* sample.

No.	RT [min]	RI determined	Area [%]	Compound name	Ref.
1	3.13	821	1.18	2-hexenal	[33]
2	5.73	1021	0.86	*p*-cymene	[34]
3	6.39	938	1.52	*α*-pinene	[34]
4	9.65	1228	0.67	cuminaldehyde	[35]
5	7.87	1034	1.48	limonene	[34,36]
6	11.60	1488	4.43	β-ionone	[34,36]
7	12.46	988	3.36	myristicin	[37]

 doi:10.20944/preprints202408.1706.v1

8	16.15	1090	0.61	linalool	[34,36]
9	17.14	1212	1.56	myrtenal	[38]
10	18.32	1843	4.51	anethole	[34]
11	19.42	1165	0.79	decanal	[39]
12	20. 09	1473	19.49	α-curcumene	[34]
13	21.43	1247	1.85	carvone	[34,36]
14	22.67	1663	3.42	apiole	[40]
15	23.39	3113	1.08	campesterol	[41]
16	25.66	4776	4.81	*n*-hentriacontane	[42]
17	27.19	1365	4.76	vanillin	[39]
18	28.81	3333	11.78	β-amirin	[43]
19	30.68	1587	3.12	spathulenol	[34]
20	32.38	1193	0.37	octyl acetate	[44]
21	36.65	3139	0.92	stigmasterol	[45]
22	37.17	3289	4.38	β-sitosterol	[45]
23	37.57	1293	2.29	germacrene D	[34,46]
24	49.57	1507	0.89	cadinene	[46]
25	55.89	1627	2.25	cadinol	[46]

GC–MS: Gas chromatography–mass spectrometry; RI: Retention index (RIs calculated based upon a calibration curve of a C8–C20 alkane standard mixture); RT: Retention time.

The GC–MS analysis illustrates 25 major compounds, constituting 82.38% of the total peak area in the *H. sphondylium* sample (Figure 1).

2.2. MS Analysis of H. sphondylium Sample

The mass spectrum shown in Figure 2 indicates the presence of multiple biomolecules detected and assigned to various chemical categories from terpenes, fatty acids, flavonoids, phenolic acids, amino acids, hydrocarbons, organic acids, esters, sterols, coumarins, iridoids, phenylpropanoids, alcohols, and miscellaneous constituents. These results corroborate the data reported in the literature [1,2,8,10,14–17,47–51].

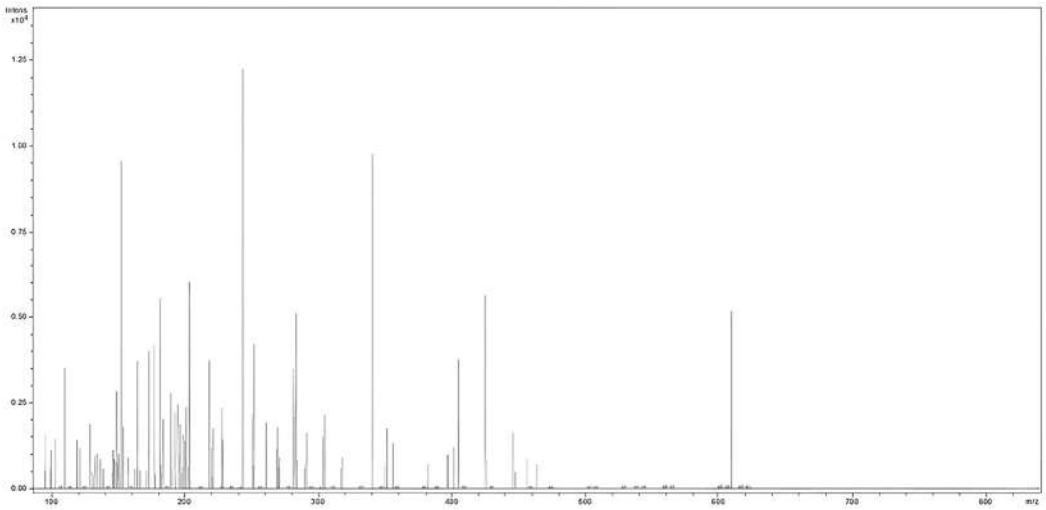

Figure 2. Mass spectrum of *H. sphondylium* sample.

Table 2 highlights the phytochemicals identified *via* electrospray ionization–quadrupole time-of-flight–mass spectrometry (ESI–QTOF–MS) analysis.

Table 2. Biomolecules identified by mass spectrometry analysis in *H. sphondylium* sample.

 doi:10.20944/preprints202408.1706.v1

No.	Detected *m/z*	Theoretical *m/z*	Molecular formula	Tentative of identification	Category	Ref.
1	76.07	75.07	$C_2H_5NO_2$	glycine	amino acids	[47]
2	90.88	89.09	$C_3H_7NO_2$	alanine	amino acids	[47]
3	106.08	105.09	$C_3H_7NO_3$	serine	amino acids	[47]
4	121.13	119.12	$C_4H_9NO_3$	threonine	amino acids	[47]
5	134.11	133.10	$C_4H_7NO_4$	aspartic acid	amino acids	[47]
6	148.12	147.13	$C_5H_9NO_4$	glutamic acid	amino acids	[47]
7	187.15	186.16	$C_{11}H_6O_3$	angelicin	coumarins	[1]
8	193.17	192.17	$C_{10}H_8O_4$	scopoletin	coumarins	[1]
9	203.17	202.16	$C_{11}H_6O_4$	xanthotoxol	coumarins	[16]
10	217.21	216.19	$C_{12}H_8O_4$	sphondin	coumarins	[16]
11	247.22	246.21	$C_{13}H_{10}O_5$	isopimpinellin	coumarins	[2]
12	271.29	270.28	$C_{16}H_{14}O_4$	imperatorin	coumarins	[1,48]
13	287.27	286.28	$C_{16}H_{14}O_5$	heraclenin	coumarins	[1,2,48]
14	305.28	304.29	$C_{16}H_{16}O_6$	heraclenol	coumarins	[1,2,48]
15	317.31	316.30	$C_{17}H_{16}O_6$	byakangelicol	coumarins	[48]
16	173.25	172.26	$C_{10}H_{20}O_2$	capric acid	fatty acids	[1]
17	201.33	200.32	$C_{12}H_{24}O_2$	lauric acid	fatty acids	[1]
18	229.37	228.37	$C_{14}H_{28}O_2$	myristic acid	fatty acids	[15]
19	255.42	254.41	$C_{16}H_{30}O_2$	palmitoleic acid	fatty acids	[15]
20	257.43	256.42	$C_{16}H_{32}O_2$	palmitic acid	fatty acids	[1]
21	271.49	270.50	$C_{17}H_{34}O_2$	margaric acid	fatty acids	[15]
22	281.39	280.40	$C_{18}H_{32}O_2$	linoleic acid	fatty acids	[1,16]
23	283.51	282.50	$C_{18}H_{34}O_2$	oleic acid	fatty acids	[1]
24	284.49	284.50	$C_{18}H_{36}O_2$	stearic acid	fatty acids	[1]
25	313.49	312.50	$C_{20}H_{40}O_2$	arachidic acid	fatty acids	[15]
26	341.59	340.60	$C_{22}H_{44}O_2$	behenic acid	fatty acids	[15]
27	271.25	270.24	$C_{15}H_{10}O_5$	apigenin	flavonoids	[8,10]
28	287.23	286.24	$C_{15}H_{10}O_6$	kaempferol	flavonoids	[8,10]
29	291.28	290.27	$C_{15}H_{14}O_6$	catechin	flavonoids	[10]
30	303.24	302.23	$C_{15}H_{10}O_7$	quercetin	flavonoids	[8,10]
31	449.41	448.40	$C_{21}H_{20}O_{11}$	astragalin	flavonoids	[1]
32	465.39	464.40	$C_{21}H_{20}O_{12}$	hyperoside	flavonoids	[1]
33	611.49	610.50	$C_{27}H_{30}O_{16}$	rutin	flavonoids	[8]
34	377.35	376.36	$C_{16}H_{24}O_{10}$	loganic acid	iridoids	[1]
35	139.11	138.12	$C_7H_6O_3$	*p*-hydroxybenzoic acid	phenolic acids	[10]
36	155.13	154.12	$C_7H_6O_4$	gentisic acid	phenolic acids	[8]
37	165.15	164.16	$C_9H_8O_3$	*p*-coumaric acid	phenolic acids	[8,10]
38	171.11	170.12	$C_7H_6O_5$	gallic acid	phenolic acids	[10]
39	181.17	180.16	$C_9H_8O_4$	caffeic acid	phenolic acids	[8,10]
40	195.18	194.18	$C_{10}H_{10}O_4$	ferulic acid	phenolic acids	[8,10]
41	355.32	354.31	$C_{16}H_{18}O_9$	chlorogenic acid	phenolic acids	[8]
42	149.19	148.20	$C_{10}H_{12}O$	estragole	phenylpropanoids	[49]
43	401.71	400.70	$C_{28}H_{48}O$	campesterol	sterols	[15]
44	413.69	412.70	$C_{29}H_{48}O$	stigmasterol	sterols	[15]
45	415.71	414.70	$C_{29}H_{50}O$	β-sitosterol	sterols	[1,15]
46	135.23	134.22	$C_{10}H_{14}$	*p*-cymene	terpenoids	[14,17]
47	137.24	136.23	$C_{10}H_{16}$	*α*-pinene	terpenoids	[14,17]
48	151.23	150.22	$C_{10}H_{14}O$	carvone	terpenoids	[49]
49	153.22	152.23	$C_{10}H_{16}O$	phellandral	terpenoids	[49]

 doi:10.20944/preprints202408.1706.v1

50	155.25	154.25	$C_{10}H_{18}O$	linalool	terpenoids	[49]
51	156.25	156.26	$C_{10}H_{20}O$	menthol	terpenoids	[49]
52	193.31	192.30	$C_{13}H_{20}O$	β-ionone	terpenoids	[49]
53	203.34	202.33	$C_{15}H_{22}$	*α*-curcumene	terpenoids	[17,50]
54	205.36	204.35	$C_{15}H_{24}$	germacrene D	terpenoids	[14,17]
55	207.36	206.37	$C_{15}H_{26}$	cadinene	terpenoids	[51]
56	221.34	220.35	$C_{15}H_{24}O$	spathulenol	terpenoids	[50]
57	223.38	222.37	$C_{15}H_{26}O$	cadinol	terpenoids	[51]
58	251.34	250.33	$C_{15}H_{22}O_3$	xanthoxin	terpenoids	[48]
59	273.51	272.50	$C_{20}H_{32}$	β-springene	terpenoids	[50]
60	427.69	426.70	$C_{30}H_{50}O$	β-amirin	terpenoids	[48]
61	149.21	148.20	$C_{10}H_{12}O$	anethole	miscellaneous	[1]
62	151.23	150.22	$C_{10}H_{14}O$	myrtenal	miscellaneous	[17]
63	153.16	152.15	$C_8H_8O_3$	vanillin	miscellaneous	[10]
64	193.22	192.21	$C_{11}H_{12}O_3$	myristicin	miscellaneous	[14]
65	223.25	222.24	$C_{12}H_{14}O_4$	apiole	miscellaneous	[2]
66	255.23	254.24	$C_{15}H_{10}O_4$	chrysophanol	miscellaneous	[1]
67	131.22	130.23	$C_8H_{18}O$	*n*-octanol	alcohols	[14]
68	117.19	116.20	$C_7H_{16}O$	heptanol	alcohols	[49]
69	75.13	74.12	$C_4H_{10}O$	butanol	alcohols	[49]
70	103.18	102.17	$C_6H_{14}O$	hexanol	alcohols	[49]
71	99.15	98.14	$C_6H_{10}O$	hexanal	aldehydes	[14,17]
72	129.22	128.21	$C_8H_{16}O$	octanal	aldehydes	[17]
73	157.25	156.26	$C_{10}H_{20}O$	decanal	aldehydes	[17]
74	145.22	144.21	$C_8H_{16}O_2$	isobutyl isobutyrate	esters	[17]
75	163.19	162.18	$C_{10}H_{10}O_2$	methyl cinnamate	esters	[1]
76	173.27	172.26	$C_{10}H_{20}O_2$	octyl acetate	esters	[14]
77	187.28	186.29	$C_{11}H_{22}O_2$	hexyl 2-methyl butanoate	esters	[17]
78	199.31	198.30	$C_{12}H_{22}O_2$	dihydrolinalyl acetate	esters	[17]
79	197.28	196.29	$C_{12}H_{20}O_2$	bornyl acetate	esters	[17]
80	201.33	200.32	$C_{12}H_{24}O_2$	octyl isobutyrate	esters	[14,17]
81	229.36	228.37	$C_{14}H_{28}O_2$	octyl hexanoate	esters	[14]
82	219.37	218.38	$C_{16}H_{26}$	5-phenyldecane	hydrocarbons	[46]
83	261.49	260.50	$C_{19}H_{32}$	4-phenyltridecane	hydrocarbons	[46]
84	353.69	352.70	$C_{25}H_{52}$	pentacosane	hydrocarbons	[1]
85	381.69	380.70	$C_{27}H_{56}$	heptacosane	hydrocarbons	[1]
86	395.81	394.80	$C_{28}H_{58}$	octacosane	hydrocarbons	[1]
87	423.79	422.80	$C_{30}H_{62}$	triacontane	hydrocarbons	[1]
88	437.81	436.80	$C_{31}H_{64}$	*n*-hentriacontane	hydrocarbons	[1]

2.3. Chemical Screening

A total of 88 biomolecules identified through MS were appointed to various categories: terpenoids (17.04%), fatty acids (12.5%), coumarins (10.22%), flavonoids (7.95%), phenolic acids (7.95%), amino acids (6.81%), phytosterols (3.40%), esters (9.09%), hydrocarbons (7.95%), alcohols (4.54%), aldehydes (3.40%), phenylpropanoids (1.13%), iridoids (1.13%), and miscellaneous. Figure 3 shows the arrangement chart bar of phytochemicals from *H. sphondylium* according to the results of MS analysis (Table 2).

 doi:10.20944/preprints202408.1706.v1

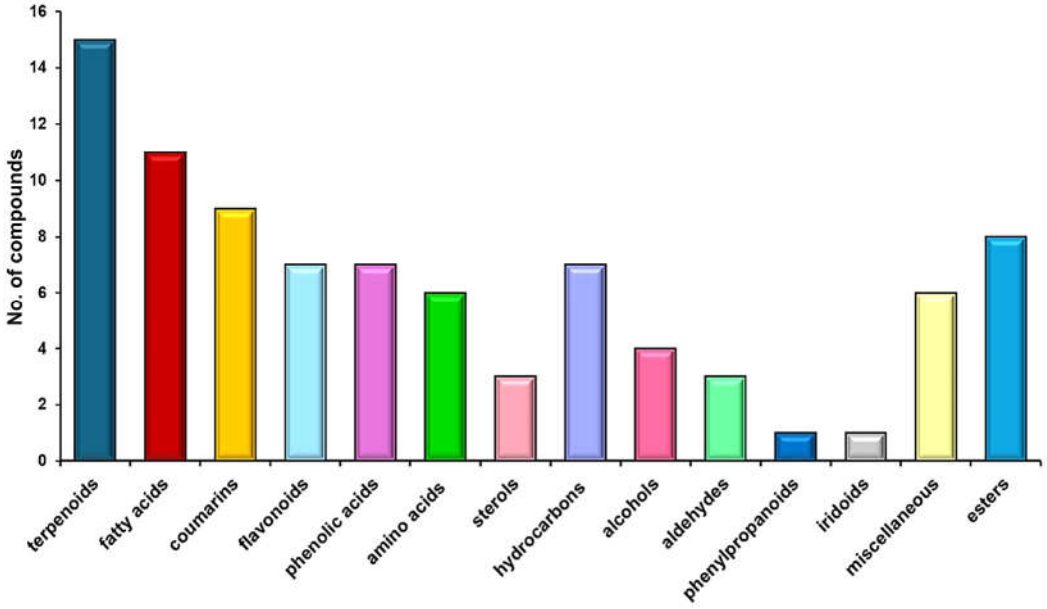

Figure 3. Phytochemicals classification bar chart of *H. sphondylium* sample.

2.4. Key Aroma-Active Compounds Forming Different Flavor Characteristics

The volatile organic compound (VOC) odor profile of biomolecules identified in *H. sphondylium* sample is presented in Table 3 and Figure 4.

Table 3. Volatile organic compounds identified *via* mass spectrometry in *H. sphondylium* sample.

Volatile organic compound	Odor profile
p-cymene	woody
α-pinene	piney
carvone	minty
phellandral	pungent, terpenic
linalool	floral, woody
menthol	minty
β-ionone	woody
α-curcumene	herbal
germacrene D	woody
cadinene	woody
spathulenol	herbal, fruity
cadinol	herbal
xanthoxin	floral
anethole	minty
myrtenal	herbal
vanillin	vanilla
myristicin	spicy
apiole	herbal
hexanal	herbal
octyl acetate	fruity
octyl butyrate	fruity
octanal	citrus
decanal	citrus
isobutyl isobutyrate	sweet
methyl cinnamate	fruity

 doi:10.20944/preprints202408.1706.v1

Volatile organic compound	Odor profile
hexyl 2-methyl butanoate	sweet, fruity
bornyl acetate	piney
octyl hexanoate	fruity, herbal

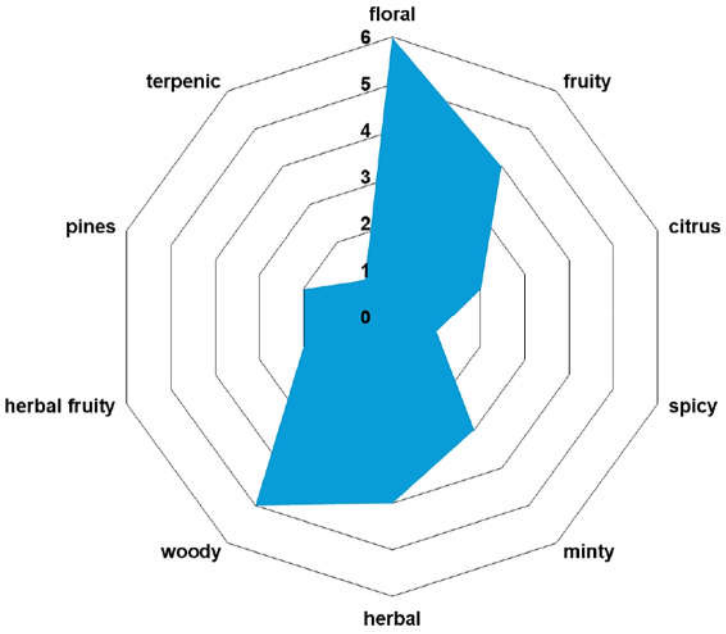

Figure 4. VOC odor profile compounds identified in *H. sphondylium* sample. VOC: Volatile organic compound.

2.5. Phytocarrier Engineered System

2.5.1. FTIR Spectroscopy

Fourier-transform infrared (FTIR) spectroscopy was utilized to examine the chemical interaction between AgNPs and phytoconstituents in plants, besides the formation of the phytocarrier system. Analysis of *H. sphondylium* sample (Figure 5; Table 4) revealed the presence of various categories of biomolecules, including terpenoids, fatty acids, flavonoids, coumarins, phenolic acids, amino acids, phytosterols, aldehydes, esters, iridoids, and phenylpropanoids.

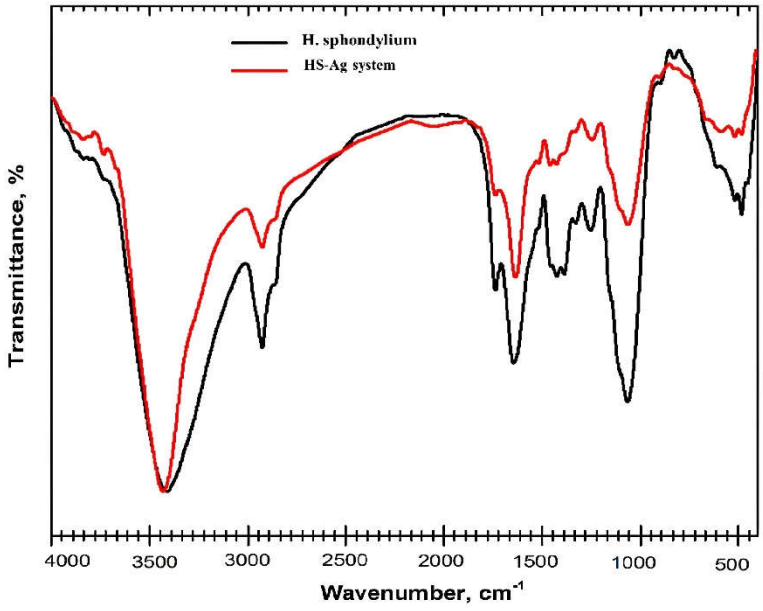

 doi:10.20944/preprints202408.1706.v1

Figure 5. FTIR spectra of *H. sphondylium* sample and HS-Ag system. FTIR: Fourier-transform infrared; HS-Ag: *H. sphondylium*–silver nanoparticles system.

Table 4. Characteristic absorption bands associated with phytoconstituents from *H. sphondylium* sample.

Biomolecules category	Wavenumber [cm^{-1}]	Ref.
terpenoids	2974, 2943, 2350, 1746, 1708, 1450, 1088, 882	[52]
coumarins	1730, 1630, 1608, 1589, 1565, 1510, 1265, 1140	[53]
flavonoids	4002–3124, 3402–3102, 1654, 1645, 1619, 1574, 1504, 1495, 1480, 1368, 1271, 1078, 768, 536	[54,55]
phenolic acids	3442, 1733, 1634, 1594, 1516, 1458, 1242, 1158, 881	[52,56]
amino acids	3400, 3332–3128, 2922, 2362, 2133, 1724–1755, 1689, 1677, 1643, 1649, 1644, 1632, 1628, 1608, 1498–1599	[52]
fatty acids	3606, 3009, 2962, 2932, 2848, 1700, 1349, 1249, 1091, 722	[36]
iridoids	1448, 1371, 1346, 1235, 1151	[57]
phytosterols	3431, 3028, 2938, 1641, 1463, 1060	[57,58]
phenylpropanoids	3188, 3002, 1636, 1504, 1449, 1248	[59]

The FTIR spectrum of the HS-Ag system exhibits characteristic vibrational bands of *H. sphondylium* sample (Figure 5). These include peaks at approximately 2922 cm^{-1} corresponding to the asymmetric vibration of the CH_2 groups from amino acids, at ~2848 cm^{-1} attributed to the symmetric vibration of the CH_2 groups from fatty acids, and at ~1746 cm^{-1} attributed to the C=O stretch of terpenoids. Additionally, the spectra show a peak at ~1644 cm^{-1} assigned to the N–H stretch of amino acids, at ~1458 cm^{-1} attributed to the aromatic ring of phenolic acids, and at ~1242, 1060, and ~1016 cm^{-1} associated with the C–N vibration of amines. Furthermore, peaks at ~882 and ~814 cm^{-1} are assigned to C–O and C–H vibrations of aromatic rings, indicating the presence of AgNPs coated with sodium citrate [32].

Nonetheless, the following vibrational peaks at ~1632, 1389, 1114, and 675 cm^{-1}, characteristic of AgNPs coated with the surfactant, exhibit observable shifts to higher wavenumbers (1642, 1392, 1118, and 681 cm^{-1}) [32,60]. The spectral shifts observed indicate the interaction between AgNPs and the O–H, C=O, N–H, and C–O functional groups of the phytochemicals present in *H. sphondylium* sample. Notable changes in the herbal sample spectra are evident, particularly in the vibrational absorption at around 3407, 1412, and 1380 cm^{-1} (O–H), besides 1292, 1150, and 1060 cm^{-1} (C–O). These shifts to higher wavenumbers suggest the involvement of these functional groups in binding the AgNPs, possibly through hydrogen bonding. Furthermore, the distinct sharpening observed in the O–H and N–H stretching regions shows distinct sharpening support evidence for HS-Ag system preparation.

2.5.2. XRD Analysis

The X-ray diffraction (XRD) patterns of *H. sphondylium* sample and HS-Ag system are shown in Figure 6.

 doi:10.20944/preprints202408.1706.v1

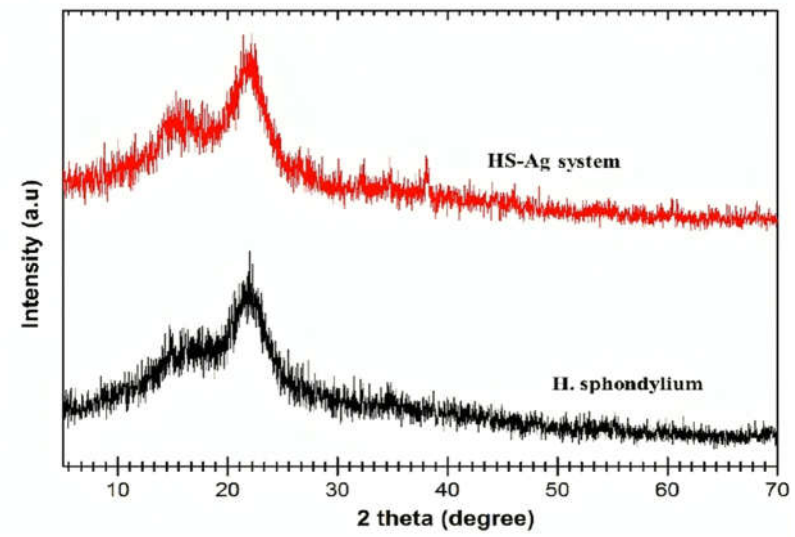

Figure 6. Powder XRD patterns of *H. sphondylium* sample and HS-Ag system. HS-Ag: *H. sphondylium*–silver nanoparticles system; XRD: X-ray diffraction.

The HS-Ag system XRD pattern displays the diffraction peaks of *H. sphondylium* biomolecules (at 2θ: 15.78° and 22.21°) and AgNPs (at 2θ: 27.87°, 38.15°, 64.4°, and 78.5°) [32,61,62].

Notably, the distinctive peaks of phytoconstituents are shifted to lower angles, indicating the incorporation of AgNPs into the herbal matrix. The interaction between AgNPs and the herbal matrix induces structural modifications, as evidenced by the discernible shift in XRD peak positions, reflecting the influential impact of metallic NPs on the herbal matrix amorphous structure.

2.5.3. SEM and EDX Analysis

Figure 7 (a and b) presents the scanning electron microscopy (SEM) images for *H. sphondylium* sample and HS-Ag system.

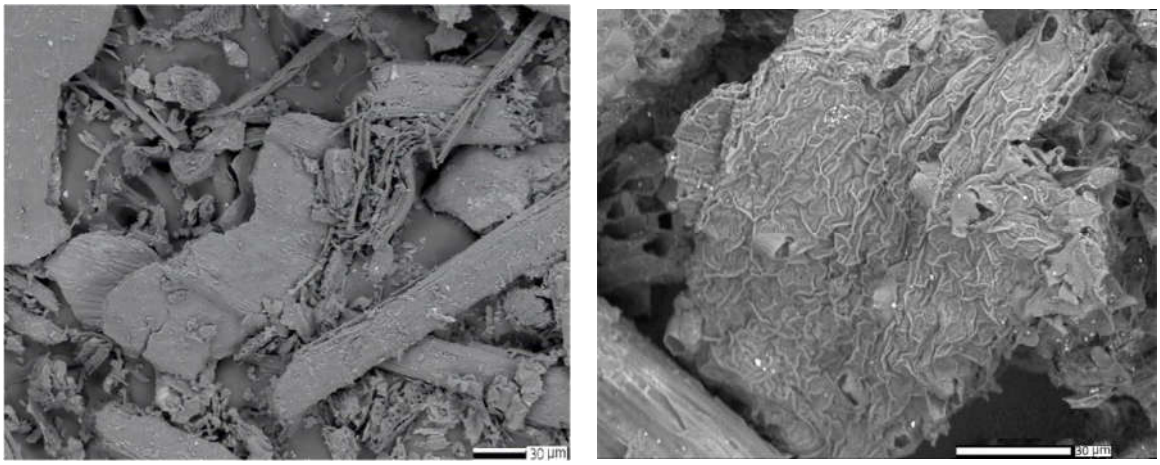

(**a**) (**b**)

Figure 7. SEM images of *H. sphondylium* sample (**a**) and HS-Ag system (**b**). HS-Ag: *H. sphondylium*–silver nanoparticles system; SEM: Scanning electron microscopy.

SEM image of *H. sphondylium* sample (Figure 7a) revealed a complex structure comprising particles of various shapes and sizes. The HS-Ag system (Figure 7b) demonstrated a modification in the morphology of *H. sphondylium* sample, with numerous nanosized spherical Ag particles (~19 nm) visibly present on the surface and within the pores of the herbal matrix particles. Moreover, the energy dispersive X-ray (EDX) spectra of the HS-Ag system showed characteristic peaks

 doi:10.20944/preprints202408.1706.v1

corresponding to both *H. sphondylium* sample and AgNPs, as depicted in Figure 8 (a and b), confirming the successful preparation of the newly engineered phytocarrier.

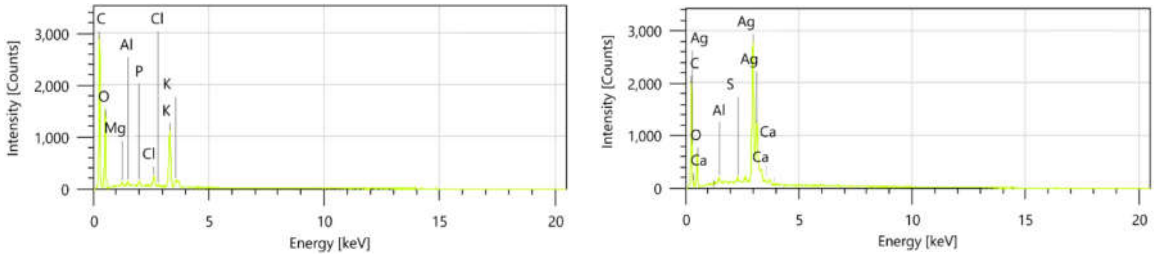

(**a**) (**b**)

Figure 8. EDX composition of *H. sphondylium* sample (**a**) and HS-Ag system (**b**). EDX: Energy dispersive X-ray; HS-Ag: *H. sphondylium*–silver nanoparticles system.

2.5.4. DLS Analysis

The study results on the stability and dynamics of herbal matrix particles and a new system obtained by the dynamic light scattering (DLS) method are shown in Figure 9 (a and b).

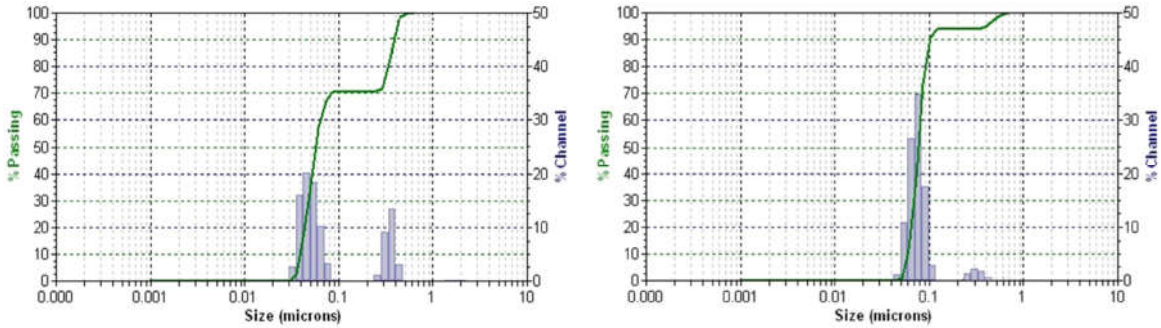

(**a**) (**b**)

Figure 9. DLS patterns of *H. sphondylium* sample (**a**) and HS-Ag system (**b**). DLS: Dynamic light scattering; HS-Ag: *H. sphondylium*–silver nanoparticles system.

The DLS profile of *H. sphondylium* sample and HS-Ag system displays two distinct peaks within a narrow range. This suggests the presence of two particle populations for each sample, with sizes of 0.049 µm and 0.36 µm for herbal matrix particles and 0.039 µm and 0.26 µm for the HS-Ag system. The narrow range of the peaks indicates high stability [63]. Additionally, the decrease in particle size in HS-AgNPs system results in a higher surface area, leading to faster and more effective dissolution than *H. sphondylium* sample.

2.6. Screening of Antioxidant Potential

To comprehensively assess the antioxidant capacity, three specific *in vitro* assays – total phenolic content (TPC), ferric reducing antioxidant power (FRAP), and 2,2-diphenyl-1-picrylhydrazyl (DPPH) – were selected. The results are illustrated in Figure 10 (a–c) and Table 5.

 doi:10.20944/preprints202408.1706.v1

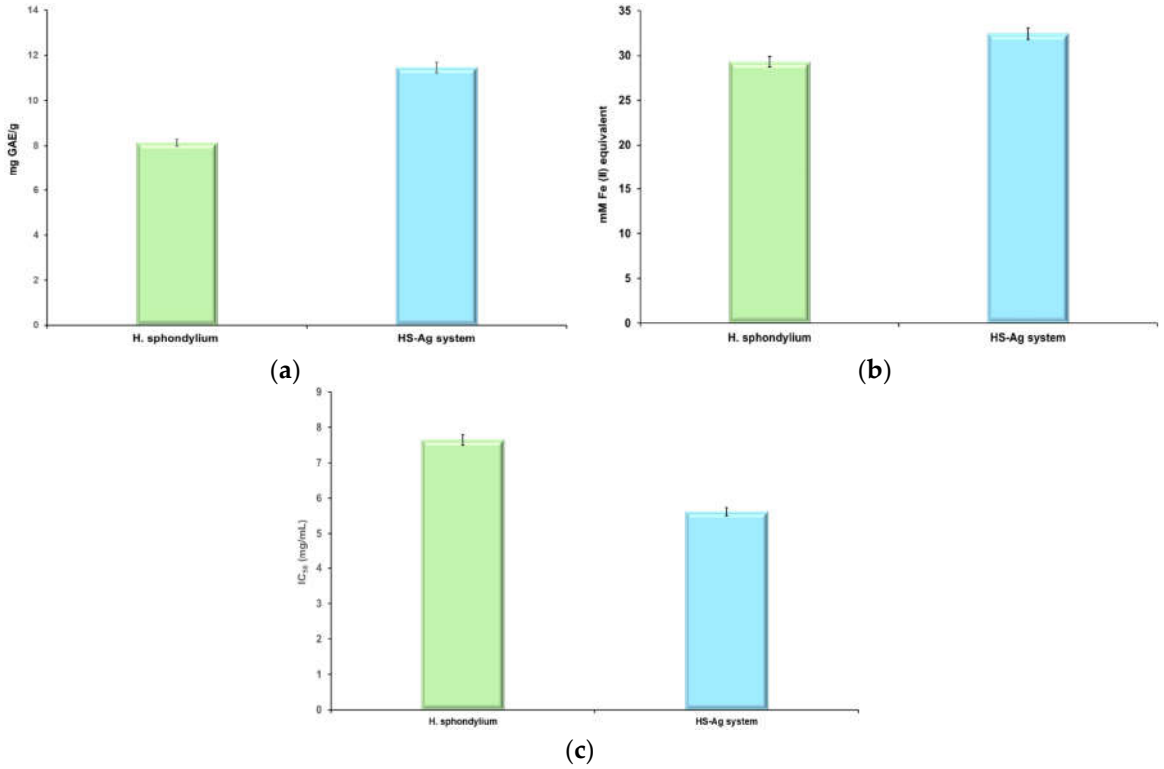

Figure 10. Graphic representation of TPC (**a**), FRAP (**b**), and DPPH (**c**) assay outcomes. DPPH: 2,2-Diphenyl-1-picrylhydrazyl; FRAP: Ferric reducing antioxidant power; GAE: Gallic acid equivalents; HS-Ag: *H. sphondylium*–silver nanoparticles system; IC_{50}: Half maximal inhibitory concentration; TPC: Total phenolic content.

Table 5. Antioxidant assays outcomes for both samples (*H. sphondylium* and HS-Ag system).

Sample	TPC [mg GAE/g]	FRAP [mM Fe^{2+}]	DPPH IC_{50} [mg/mL]
H. sphondylium	8.14±0.18	29.31±0.11	7.65±0.05
HS-Ag system	11.47±0.16	32.44±0.08	5.62±0.07

Values are expressed as the mean ± SD (n=3). DPPH: 2,2-Diphenyl-1-picrylhydrazyl; FRAP: Ferric reducing antioxidant power; GAE: Gallic acid equivalents; IC50: Half maximal inhibitory concentration; TPC: Total phenolic content.

The findings from the TPC assay indicate a substantial rise in phenolic content (40.91%) in the HS-Ag system compared to *H. sphondylium*, which is attributed to the catalytic properties of AgNPs [64]. The FRAP assay data also demonstrates a moderate increase (10.67%) in reducing power for the HS-Ag system over *H. sphondylium*. Furthermore, the DPPH radical scavenging assay results reveal a significant decrease (26.53%) in the half maximal inhibitory concentration (IC_{50}) value for scavenging activity associated with a higher antioxidant activity.

2.7. Antimicrobial Screening

The screening of antimicrobial activity against selected pathogenic microorganisms was tested in this study, specifically against *Staphylococcus aureus* (Gram-positive), *Bacillus subtilis* (Gram-positive), *Pseudomonas aeruginosa* (Gram-negative), and *Escherichia coli* (Gram-negative), using the agar well diffusion method. *H. sphondylium* and a newly prepared HS-Ag system were evaluated for their antibacterial activity by measuring the diameter of inhibition zones (IZs) and comparing the results with positive (Gentamicin) and negative (dimethyl sulfoxide – DMSO) controls. The data presented in Table 6 indicates that both samples (*H. sphondylium* and HS-Ag system) exhibited strong antibacterial activity against all tested pathogenic microorganisms.

 doi:10.20944/preprints202408.1706.v1

Table 6. Results of antibacterial activity against selected pathogenic microorganisms.

Pathogenic microorganism	Sample	Inhibition zone diameter [mm]						
		Sample concentration [µg/mL]					*Positive control (Gentamicin 100 µg/mL)*	*Negative control (DMSO)*
		100	*125*	*150*	*175*	*200*		
Staphylococcus aureus	*H. sphondylium*	11.23±0.75	13.98±1.17	17.06±0.68	21.19±0.72	25.46±0.45	9.57±0.35	0
	HS-Ag system	14.78±0.54	17.27±0.78	21.62±0.47	28.52±0.56	34.14±0.56		
Bacillus subtilis	*H. sphondylium*	19.83±0.09	21.47±0.43	24.36±0.32	27.69±0.38	31.22±0.31	17.89±0.28	0
	HS-Ag system	23.11±0.41	25.38±0.36	29.51±0.16	32.76±0.47	36.25±0.28		
Pseudomonas aeruginosa	*H. sphondylium*	10.64±0.27	14.09±0.21	16.73±0.25	18.95±0.82	20.38±0.17	18.67±0.19	0
	HS-Ag system	21.78±0.19	23.01±0.17	24.74±0.32	26.18±0.61	27.65±0.19		
Escherichia coli	*H. sphondylium*	11.84±0.37	14.69±0.34	17.15±0.51	19.03±0.43	21.49±0.34	20.69±0.31	0
	HS-Ag system	20.88±0.28	21.63±0.25	23.06±0.42	25.02±0.47	27.12±0.58		

Values are expressed as the mean ± SD (*n*=3). DMSO: Dimethyl sulfoxide; HS-Ag: *H. sphondylium*–silver nanoparticles system; SD: Standard deviation.

Notably, even at the lowest concentration tested (100 µg/mL), both the herbal sample and HS-Ag system showed significantly higher IZ than positive control (Gentamicin) against both Gram-positive bacteria strains (*S. aureus* and *B. subtilis*). However, for the Gram-negative bacteria strains, the antibacterial IZs obtained for the lowest concentration of the herbal sample (100 µg/mL) were lower than Gentamicin (43.01% against *P. aeruginosa* and 44.77% against *E. coli*). Conversely, the lower concentration (100 µg/mL) of HS-Ag system displays a slightly larger IZ diameter than Gentamicin against *P. aeruginosa* (16.65%). Meanwhile, the antibacterial IZs against *E. coli* obtained for the same concentration of HS-Ag system (100 µg/mL) are almost similar (20.88±0.28 mm) to Gentamicin (20.69±0.31 mm).

The highest concentrations of herbal sample and HS-Ag system (200 µg/mL) demonstrated the largest IZ diameters against *S. aureus*, *B. subtilis*, *P. aeruginosa*, and *E. coli*. Additionally, the HS-Ag system was more effective at inhibiting the growth of all tested bacterial strains at all concentrations than *H. sphondylium*.

To confirm the antibacterial efficacy of samples (*H. sphondylium* and the newly formulated HS-Ag system), the minimum inhibitory concentration (MIC) and minimum bactericidal concentration (MBC) were determined against all bacterial strains. The results are illustrated in Table 7.

Table 7. MICs and MBCs of samples against selected pathogenic microorganisms.

Pathogenic microorganism	Sample	MIC [µg/mL]	MBC [µg/mL]	Gentamicin	
				MIC [µg/mL]	*MBC [µg/mL]*
Staphylococcus aureus	*H. sphondylium*	0.22±0.07	0.23±0.19	0.62±0.22	0.62±0.21
	HS-Ag system	0.12±0.03	0.11±0.16		
Bacillus subtilis	*H. sphondylium*	0.28±0.19	0.24±0.12	0.49±0.18	0.43±0.19
	HS-Ag system	0.16±0.08	0.15±0.23		
Pseudomonas aeruginosa	*H. sphondylium*	0.98±0.11	0.99±0.14	1.27±0.16	1.26±0.19
	HS-Ag system	0.52±0.07	0.59±0.37		
Escherichia coli	*H. sphondylium*	0.38±0.09	0.31±0.21	0.82±0.19	0.82±0.17
	HS-Ag system	0.26±0.13	0.26±0.15		

Values are expressed as the mean ± SD (*n*=3). HS-Ag: *H. sphondylium*–silver nanoparticles system; MBC: Minimum bactericidal concentration; MIC: Minimum inhibitory concentration; SD: Standard deviation.

Both samples demonstrated significant antimicrobial activity in MIC and MBC assays. The MIC value of *H. sphondylium* sample varies from 0.22±0.07 to 0.98±0.11 µg/mL, while for the HS-Ag system from 0.12±0.03 to 0.52±0.07 µg/mL, respectively. Correspondingly, the MBC values for both investigated samples aligned closely with the MIC values. These results demonstrated a superior antibacterial effect of the HS-Ag system compared to herbal sample across all bacterial strains tested.

 doi:10.20944/preprints202408.1706.v1

It's worth noting that the MIC and MBC values for both samples are lower than those of Gentamicin (positive control). The bacterial growth was absent in the negative control, which only contained nutrient broth.

2.8. Cell Viability Assay

Figure 11 (a and b) illustrates the results of cell viability testing using 3-(4,5-dimethylthiazol-2-yl)-2,5-diphenyltetrazolium bromide (MTT) assay on *H. sphondylium* and HS-Ag system samples at various concentrations (75, 100, 125, 150, 175, and 200 µg/mL).

The data suggests that lower concentrations of *H. sphondylium* correspond to higher cell viability, indicating a less toxic effect on the normal human dermal fibroblasts (NHDF) cell line. A constant, slight decrease in cell viability was observed within the 75–150 µg/mL concentration range. At higher concentrations of 175 and 200 µg/mL, a more significant decrease in cell viability occurred, but it remained above 74% (Figure 11a).

In the case of the cervical cancer (Henrietta Lacks – HeLa) cell line, there was a consistent decrease in cell viability as the concentration of the herbal extract increased. The most notable impact occurs at higher concentrations (175 and 200 µg/mL) (Figure 11b).

Similarly, in the case of the HS-Ag system, the outcomes of the MTT assay indicated that cell viability was dose-dependent. Thus, the NHDF cells display a continuous decrease in cell viability when the HS-Ag system concentration increases. Notably, at 200 µg/mL, the maximum concentration of the HS-Ag system corresponds to the lower cell viability value (70.46 µg/mL) but remains above the standard value (Figure 11a).

However, the HS-Ag system had a notably more pronounced negative impact on the HeLa tumor cell line, with an inversely proportional relationship between concentration and cell viability. Specifically, the maximum effect of 50.26% was observed at 200 µg/mL of the HS-Ag system (Figure 11b).

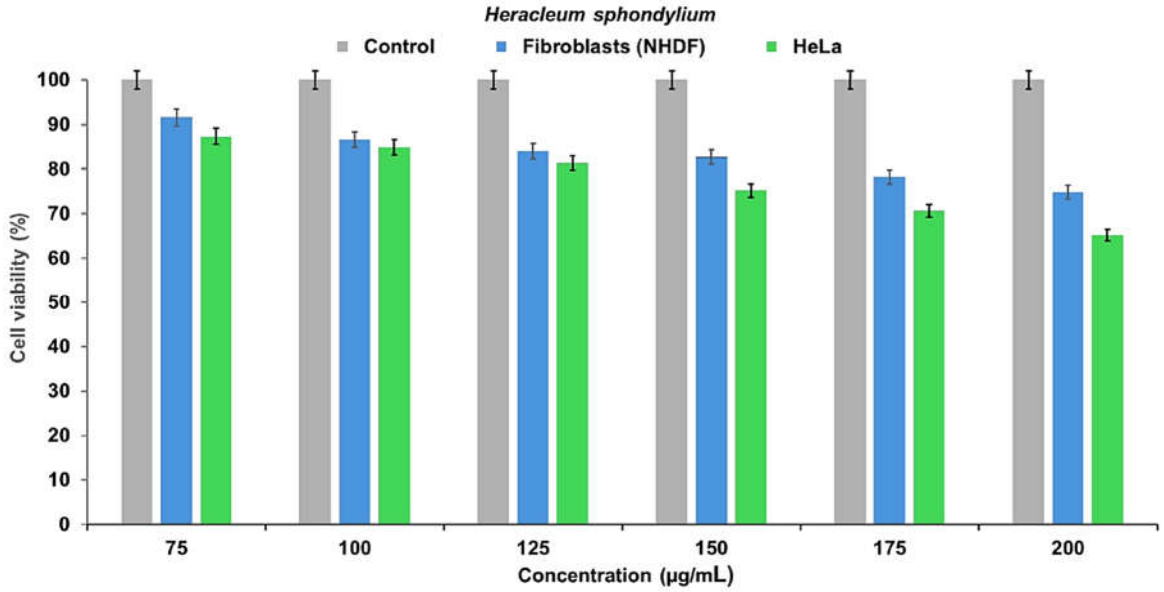

(**a**)

 doi:10.20944/preprints202408.1706.v1

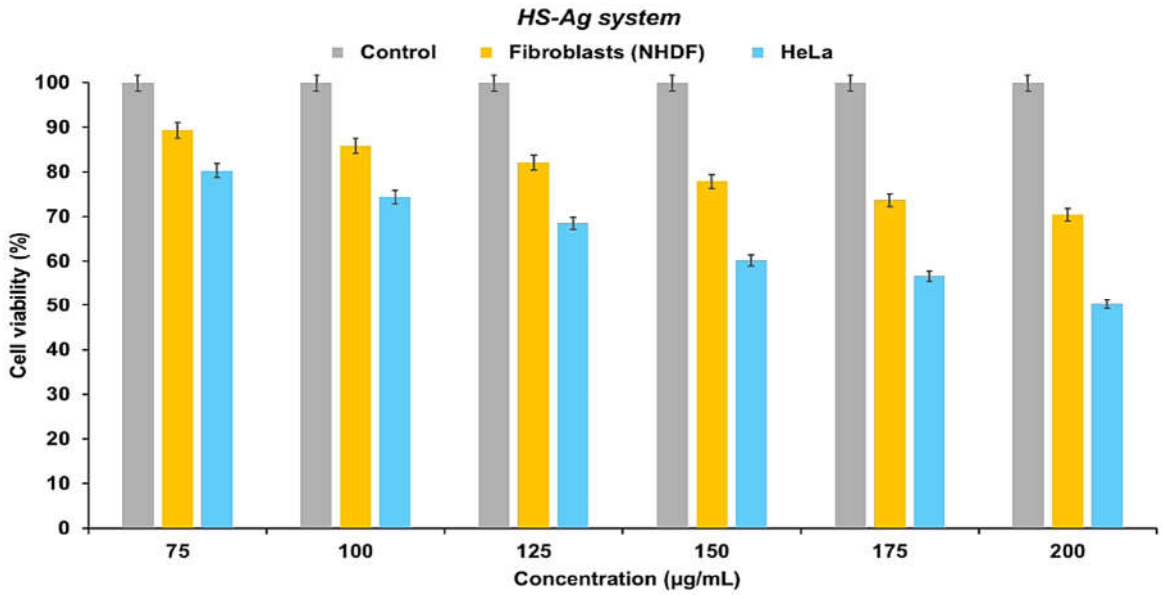

(**b**)

Figure 11. Viability of NHDF and HeLa cells, 24 hours after co-incubation with different concentrations of *H. sphondylium* sample (**a**) and HS-Ag system (**b**). Positive control wells contained untreated cells, MTT solution, and DMSO. Data are represented as mean ± SEM of three independent readings (*n*=3). DMSO: Dimethyl sulfoxide; HeLa: Henrietta Lacks; HS-Ag: *H. sphondylium*–silver; MTT: 3-(4,5-Dimethylthiazol-2-yl)-2,5-diphenyltetrazolium bromide; NHDF: Normal human dermal fibroblasts; SEM: Standard error of the mean.

The IC_{50} values of *in vitro* cytotoxicity calculated for *H. sphondylium* are higher than those for the HS-Ag system, as illustrated in Figure 12.

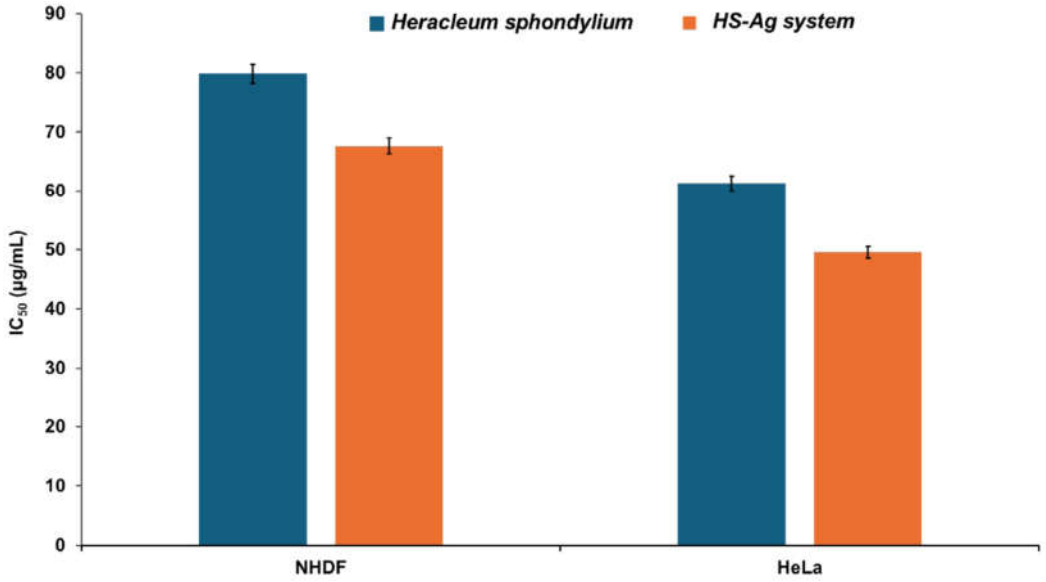

Figure 12. *In vitro* cytotoxicity of HS-Ag system *vs. H. sphondylium*, as a function of concentration against NHDF and HeLa cell lines (after 24 hours). Data are represented as mean ± SEM of three independent readings (*n*=3). HeLa: Henrietta Lacks; HS-Ag: *H. sphondylium*–silver nanoparticles system; IC_{50}: Half maximal inhibitory concentration; NHDF: Normal human dermal fibroblasts; SEM: Standard error of the mean.

 doi:10.20944/preprints202408.1706.v1

Thus, for NHDF cells, the IC_{50} values of *H. sphondylium* and HS-Ag system were 79.82±0.023 and 67.65±0.019 μg/mL, respectively. For HeLa cells, the IC_{50} values of *H. sphondylium* and HS-Ag system were 61.31±0.078 and 49.54±0.064 μg/mL, respectively. The data suggests that the HS-Ag system exhibits higher cytotoxicity than *H. sphondylium* against tumor cells (19.18%).

3. Discussion

H. sphondylium, a renowned medicinal plant with well-established therapeutic properties in Romanian ethnomedicine, has gained recent attention due to its remarkable biological activity. The escalating concerns surrounding antimicrobial resistance led to a critical reevaluation of current therapeutic strategies for infectious diseases. Recent research focuses on the new selective targeting strategies for innovative antimicrobial agents. Special attention is paid to new efficient antibiotics based on medicinal plants and nanotechnology.

3.1. H. sphondylium Low-Metabolic Profile

Concerning *H. sphondylium* low-metabolic profile, a total of 88 biomolecules were detected through GC–MS and ESI–QTOF–MS, encompassing a diverse array of categories, mainly terpenoids, coumarins, flavonoids, phenolic acids, amino acids, fatty acids, phytosterols, phenylpropanoids, iridoids.

Terpenoids represent over 17% of the total *H. sphondylium* phytoconstituents (Figure 3). The therapeutic properties of terpenoids are multiple, including anti-inflammatory, antimicrobial, antiviral, antitumor, analgesic, cardioprotective, antispastic, antihyperglycemic, and immunomodulatory [65].

Coumarins are the second class of metabolites, representing over 10% of the phytochemicals from the hogweed sample (Figure 3). Research has reported that these secondary metabolites possess high antioxidant, antiviral, anti-inflammatory, antitumor, neuroprotective, anticoagulant, anticonvulsant, cardioprotective, antihypertensive, immunomodulatory, and antidiabetic properties [54,66].

Flavonoids, which comprise approximately 8% (Figure 3), are metabolites with outstanding biological activities: antimicrobial, antioxidant, cardioprotective, antiviral, neuroprotective, and antitumor [67].

Phenolic acids represent a significant class of phytochemicals identified in the composition of *H. sphondylium* sample (Figure 3). Research showed that these metabolites exhibit anti-inflammatory, antibacterial, antioxidant, antidiabetic, anti-allergic, antitumor, cardioprotective, and neuroprotective properties [68,69].

Amino acids are another category of phytochemicals encompassing over 83% of non-essential amino acids (glycine, alanine, serine, aspartic acid, glutamic acid) (Figure 3). About 50% of these compounds (glycine, alanine, glutamic acid) exert antiproliferative and immunomodulatory activity. Over 33% (serine and threonine) act as anti-inflammatory agents. In addition, studies report the beneficial effect of aspartic acid on neurological and psychiatric diseases [70,71].

Fatty acids comprise 12.5% of total phytochemicals from the *H. sphondylium* sample, with about 72% saturated fatty acids (capric, stearic, behenic, lauric, myristic, margaric, arachidic, and palmitic acids), two monosaturated fatty acids (oleic and palmitoleic acids) and one ω-6 acid (linoleic acid) (Table 2; Figure 3). These compounds possess anti-inflammatory, antioxidant, antimicrobial, neuroprotective, and cardioprotective properties [72].

Phytosterols represent over 3% of the total phytochemicals (Figure 3) and act as antioxidant, neuroprotective and cardioprotective, anti-inflammatory, antitumor, immunomodulatory agents [73].

The phenylpropanoid estragole (Table 2) displays antibacterial, antiviral, antioxidant, anti-inflammatory, and immunomodulatory activity [74].

Iridoid compound loganic acid (Table 2) possesses neuroprotective, anti-inflammatory, antioxidant, and antiadipogenic effects [75].

 doi:10.20944/preprints202408.1706.v1

3.2. New Phytocarrier System with Antioxidant, Antimicrobial and Cytotoxicity Potential

The utilization of nanotechnology and the advancement of engineered delivery systems employing metallic NPs circumvent the *in vitro* deficiencies, particularly stability, and reduced adsorption, associated with certain phytoconstituents possessing heightened biological activity. These tailored systems promote targeted activity, prolonged drug release, reduced drug doses, and lowered toxicity. Additionally, they can improve the therapeutic effects by combining the actions of the herbal compounds and the metallic NPs [22,23,76]. As a result, a new delivery system based on AgNPs was developed from *H. sphondylium*.

Multiple assays provide a thorough and precise evaluation of the antioxidant potential of herbal products. *In vitro* tests are particularly valuable for assessing the antioxidant activity of samples containing complex compositions of biomolecules. The antioxidant activity of *H. sphondylium* is linked intricately to the highly active phytoconstituents. Conversely, the antioxidant potential within the HS-Ag system is derived from the phytochemicals and AgNPs conjugate effect. The results suggest that in the HS-Ag system, AgNPs, in conjunction with the phytoconstituents, could act as hydrogen donors, reducing agents, and singlet oxygen quenchers [77].

The results suggest that the antimicrobial efficacy of both samples is dose-dependent, consistent with existing literature [78]. Gram-positive bacterial strains (*S. aureus* and *B. subtilis*) exhibited a greater sensitivity to both *H. sphondylium* and HS-Ag system samples compared to Gram-negative bacteria (*P. aeruginosa* and *E. coli*), possibly attributed to morphological variances within these distinct microorganism categories. Additionally, the outer membrane features of Gram-negative bacteria may act as a barrier against various compounds [79].

The antimicrobial activity of *H. sphondylium* sample can be attributed to its complex mixture of phytoconstituents renowned for their antimicrobial properties, encompassing flavonoids, terpenoids, phenolic acids, fatty acids, and phenylpropanoids (estragole, anethole, myristicin) [80,81].

Notably, phenolic acids impact the bacterial membrane and cytoplasmic levels, while flavonoids act on the membrane level and inhibit deoxyribonucleic (DNA) and ribonucleic (RNA) synthesis [69]. Furthermore, terpenoids restrict bacterial respiration and oxidative phosphorylation [82,83].

Conversely, the antimicrobial activity of the HS-Ag system may be ascribed to the synergistic biological mechanism of phytochemicals and AgNPs. While the biological mechanism of AgNPs remains elusive, numerous studies have reported that AgNPs disrupt membrane interactions and adversely impact bacterial DNA [32].

The lower values of the MIC and MBC are associated with the most efficient antimicrobial effect [79]. The *H. sphondylium* sample displayed the lowest MIC values against *B. subtilis*, followed by *S. aureus*, *E. coli*, and *P. aeruginosa*. The bacterial susceptibility diversity could be associated either with their resistance or the sample composition, specifically with the conjugate antimicrobial effect of different categories of phytoconstituents in the case of *H. sphondylium*, multiplied by the presence of AgNPs in HS-Ag system [79]. Furthermore, all bacteria employed in this study are associated with various infections. Research has demonstrated that Gram-negative microorganisms are reservoirs for hospital-acquired infections, and there is a growing concern regarding drug-resistant infections attributable to Gram-negative bacteria [84]. Hence, the findings from this study advocate the potential utilization of the newly formulated HS-Ag system as an antimicrobial agent.

In vitro cytotoxicity assays are commonly employed to assess the potential toxicity of a specific compound on cell culture models. These assays ascertain the impact of the compound on cell viability, growth, morphology, and metabolism, as well as its ability to impede cell viability, cell growth, and proliferation, offering insights into its cytotoxicity as an initial step in bioavailability assessment. Among the various methods available, colorimetric assays, particularly the MTT assay, are widely utilized, considering their cost-effectiveness *in vitro* cell viability assessment [85–87]. The findings suggest that the herbal extract and the newly prepared engineered phytocarrier are not toxic to the NHDF cell line [87]. In the case of the cervical cancer (HeLa) cell line, a significant decrease in cell viability as the concentration of the herbal extract increased (175 and 200 µg/mL) was highlighted. Also, the results support the existing reported data [1]. Moreover, the HS-Ag system exhibited higher

 doi:10.20944/preprints202408.1706.v1

cytotoxicity than *H. sphondylium* against the tumor cell line. This finding could be attributed to the synergistic effects of phytoconstituents and the ability of AgNPs to facilitate the generation of reactive oxygen species [88].

4. Materials and Methods

4.1. Chemicals and Reagents

All used reagents were analytical grade. Ethanol, methanol, dichloromethane, chloroform, sodium carbonate, gallic acid, DPPH, acetate buffer solution (pH 4–7), FRAP assay kit (MAK369-1KT), and DMSO were acquired from Sigma Aldrich (München, Germany) and used without further purification. MTT kit was obtained from AAT Bioquest (Pleasanton, CA, USA). Ultrapure water was used in all experiments.

4.2. Cell Lines

NHDF and HeLa cell lines were purchased from the American Type Culture Collection (ATCC; Manassas, VA, USA). Both cell lines were cultivated at 37°C, in Dulbecco's Modified Eagle's Medium (DMEM; Gibco, Life Technologies, Leicestershire, UK), supplemented with 10% fetal bovine serum (FBS), and 1% antibiotic antimycotic solution (Sigma Aldrich).

4.3. Bacterial Strains

S. aureus (ATCC 29213), *B. subtilis* (ATCC 9372), *P. aeruginosa* (ATCC 27853), and *E. coli* (ATCC 25922) were purchased from the ATCC (Manassas, VA, USA).

4.4. Plant Material

The *H. sphondylium* samples (whole plant – stems of 165 cm in height, leaves, flowers of 25 cm diameter, and roots) were collected in June 2022 from the area of Timiş County, in Western Romania (geographic coordinates 45°43′02″ N, 21°19′31″ E) and taxonomically authenticated at the West University of Timişoara. Voucher specimens (HERA-SPD-2022-0806) were deposited at the Department of Pharmaceutical Botany, Faculty of Pharmacy, University of Medicine and Pharmacy of Craiova, Romania.

4.5. Preparation of AgNPs

AgNPs were prepared according to a procedure described in our previous paper [32].

4.6. Plant Sample Preparation for Chemical Screening

The freeze-dried plant samples (whole plant) were milled using a planetary Fritsch Pulverisette mill (Idar-Oberstein, Germany), 720 rpm for 12 minutes at 24°C, then sieved through American Society for Testing Materials (ASTM) standard test sieve series to obtain particles of 0.25–0.30 mm range. The vegetal material was subject to sonication extraction (Elmasonic, Singen, Germany) for 50 minutes at 45°C and 65 Hz dissolved in methanol (20 mL). All extracts were prepared in triplicate.

4.7. GC–MS Analysis

GC analysis was performed using the GCMS-QP2020NX Shimadzu equipment provided with a ZB-5MS capillary column (30 m length, 0.25 mm inner diameter, 0.25 μm film thickness) from Agilent Technologies (Santa Clara, CA, USA). Helium was used as the carrier gas at a flow rate of 1 mL/min.

4.7.1. GC–MS Separation

The oven temperature program was initiated at 50°C, held for 2 minutes, and subsequently ascended to 300°C at a rate of 5°C per minute, where it was maintained for 4 minutes. The injector's temperature was registered at 280°C, while the interface temperature at 225°C. Compound mass was

 doi:10.20944/preprints202408.1706.v1

measured at an ionization energy of 70 eV, commencing after a 2-minute solvent delay. The mass spectrometer source and MS Quad were maintained at 225°C and 160°C, respectively. The compounds' identification was accomplished based on their mass spectra, compared with the USA National Institute of Standards and Technology (NIST) 2.0 software (NIST, Gaithersburg, MD, USA) database, and supplemented with a literature review.

4.7.2. Mass Spectrometry

The MS experiments were carried out using an ESI–QTOF–MS analysis system (Bruker Daltonics, Bremen, Germany). The mass spectra were acquired in the positive ion mode over a mass range of 100 to 3000 *m*/*z*, with a scan speed of 2.0 scans per second, a collision energy ranging from 25 to 85 eV, and a source block temperature set at 85°C. Identification of phytoconstituents relied on the standard library NIST/National Bureau of Standards (NBS)-3 (NIST, Gaithersburg, MD, USA). The obtained mass spectra values and the identified secondary metabolites are shown in Table 2.

4.8. Phytocarrier System Preparation (HS-Ag System)

The HS-Ag system was prepared by mixing *H. sphondylium* (solid herb samples prepared as previously described) with an AgNPs solution in a 1:3 mass ratio. The obtained mixture was filtered (F185 mm filter paper) and dried in an oven at 40°C for 6 hours. Each experiment was carried out in triplicate.

4.9. Characterization of HS-Ag System

4.9.1. FTIR Spectroscopy

Data collection was conducted after 30 recordings at a resolution of 4 cm^{-1}, in the range of 4000-400 cm^{-1}, on Shimadzu AIM-9000 spectrometer with attenuated total reflectance (ATR) devices (Shimadzu, Tokyo, Japan).

4.9.2. XRD Spectroscopy

The X-ray powder diffraction (XRD) was carried out on a Bruker AXS D8-Advance X-ray diffractometer (Bruker AXS GmbH, Karlsruhe, Germany), CuKα radiation, *k* 0.1541 nm, equipped with a rotating sample stage, Anton Paar TTK low-temperature cell (-180°C to 450°C), high vacuum, inert atmosphere, and relative humidity control, Anton Paar TTK high-temperature cell (up to 1600°C). The XRD patterns were compared with those from the International Centre for Diffraction Data (ICDD) Powder Diffraction Database (ICDD file 04-015-9120). The average crystallite size and the phase content were determined using the whole-pattern profile-fitting (WPPF) method.

4.9.3. SEM Analysis

SEM micrographs were captured utilizing an SEM–energy dispersive X-ray spectroscopy (EDS) system (Quanta Inspect F50; FEI-Philips, Eindhoven, The Netherlands) equipped with a field-emission gun (FEG), providing a resolution of 1.2 nm. Additionally, the system incorporates an EDX spectrometer, with an MnK resolution of 133 eV.

4.9.4. DLS Particle Size Distribution Analysis

DLS analysis was conducted on a Microtrac/Nanotrac 252 (Montgomeryville, PA, USA). Each sample was analyzed in triplicate at room temperature (22°C) at a scattering angle of 172°.

4.10. Antioxidant Activity

The antioxidant activity of *H. sphondylium* sample and HS-Ag system was evaluated using three different methods: TPC (Folin–Ciocalteu assay), FRAP and DPPH. All experiments for antioxidant activity screening were performed in triplicate.

 doi:10.20944/preprints202408.1706.v1

4.10.1. Sample Preparation

Separately, 0.22 g of *H. sphondylium* sample and 0.22 g of HS-Ag system were added to 6 mL of 70% ethanol. Following a 10-hour stirring period at room temperature (23°C), the mixtures were centrifuged at 5000 rpm for 8 minutes. The resulting supernatant was collected for further evaluation of the antioxidant potential of each sample.

4.10.2. Determination of TPC

The TPC of *H. sphondylium* and HS-Ag system samples prepared as stated above (*vide supra*) was determined spectrophotometrically (FLUOstar Optima UV-Vis spectrometer; BMG Labtech, Offenburg, Germany) according to the Folin–Ciocalteu procedure adapted from our earlier publication [64]. The results were expressed in gallic acid equivalents (mg GAE/g sample). Sample concentrations were calculated based on the linear equation (1) obtained from the standard curve and the correlation coefficient (R^2=0.9997):

$$y=0.0021x+0.1634 \quad (1)$$

4.10.3. FRAP Assay

The FRAP antioxidant activity of *H. sphondylium* and HS-Ag system samples was determined spectrophotometrically (FLUOstar Optima UV-Vis spectrometer; BMG Labtech) at 595 nm, using a FRAP Assay Kit. The results were expressed in mM Fe^{2+}, calculated according to equation (2):

$$FRAP = \frac{mMFe^{2+} \times F_D}{V} \quad (2)$$

where *FRAP*: Ferric reducing antioxidant power; $mMFe^{2+}$: Iron ions (Fe^{2+}) amount generated from the calibration curve of each sample (mM); F_D: Dilution factor; *V*: Volume of each sample (µL).

4.10.4. DPPH Radical Scavenging Assay

The DPPH radical scavenging activity of *H. sphondylium* and HS-Ag system samples was performed according to the procedure described in our earlier publication [64]. The absorbance (*A*) was recorded at 520 nm (FLUOstar Optima UV-Vis spectrometer; BMG Labtech). The IC_{50} values (µg/mL) were determined from the inhibition percentage, *Inh(%)*, from the calibration curve generated for each sample, according to equation (3):

$$Inh(\%) = \frac{(A_0 - A_1)}{A_0} \times 10 \quad (3)$$

4.11. Antimicrobial Test

Agar well diffusion assay, MICs, and MBCs were conducted to evaluate the antimicrobial activity of *H. sphondylium* and HS-Ag system.

MICs and MBCs were determined using the microbroth dilution method (Mueller–Hinton medium). MIC was considered the lowest compound concentration that inhibits bacterial growth, while MBC represents the lowest concentration at which no visible bacterial growth occurs after 14-hour incubation. The microorganism growth inhibition was evaluated as the optical density at 600 nm using a T90+ UV–Vis spectrophotometer (PG Instruments, Lutterworth, UK) [89].

Nutrient agar and nutrient broth were prepared according to the manufacturer's instructions and autoclaved at 120°C for 20 minutes. The final concentration of microorganisms was adjusted to 0.5 McFarland Standard (1.5×10^8 CFU/mL; CFU: Colony-forming unit). Each assay was performed in triplicate [89].

The diluted sections of five concentrations (100, 125, 150, 175, and 200 µg/mL) were prepared using 25% DMSO [89].

 doi:10.20944/preprints202408.1706.v1

The antimicrobial potential of *H. sphondylium* and HS-Ag system was evaluated using the agar well diffusion method according to the experimental procedure adapted from the literature [79,90,91].

The bacterial strains were initially cultured on a nutrient substrate and then inoculated for 24 hours. Circular wells were created using a sterile glass capillary (5 mm). The bacterial strains (4–6 hours) were streaked onto the nutrient agar using a sterile swab, and this process was repeated three times, with the plate rotated between each streaking. Next, 1 mL from each sample (*H. sphondylium* and HS-Ag system) concentration was introduced into the designated wells. The plates were then placed in an incubator at 37°C for 24 hours and later analyzed to determine the IZs. DMSO served as the negative control, while Gentamicin (100 µg/mL) was used as the positive control. The diameter (mm) of the IZs around the discs was measured using a ruler to determine the extent of bacterial growth inhibition. Each assay was performed in triplicate [79,90].

4.12. Cell Culture Procedure

4.12.1. Cell Culture and Treatment

The cell lines utilized in this study included NHDF and HeLa cells (ATCC; Manassas, VA, USA). The cells were cultured at 37°C under 5% carbon dioxide (CO_2) and 100% humidity in DMEM supplemented with FBS and 1% antibiotic antimycotic solution. After seeding the cells at a density of 4×10^3 cells/well in 96-well plates, they were allowed to reach 90% confluency over 24 hours. Subsequently, the culture medium was replaced with a fresh medium containing varying concentrations (75, 100, 125, 150, 175, and 200 µg/mL) of *H. sphondylium* and HS-Ag system. The cells were then cultured for an additional 24 hours. A control group with fresh standard medium and positive and negative controls was included in the 96-well culture plate (eight wells for each test material). The experiments were conducted in triplicate, and cell viability was assessed following a 24-hour incubation at 37°C under 5% CO_2.

4.12.2. MTT Assay

The test materials were aspirated from each well of the initial plate. Subsequently, 25 µL of MTT reagent was pipetted into each well and incubated for 2 hours at 37°C in a CO_2 incubator. Subsequently, the formazan crystals formed were solubilized using DMSO. The absorbance of the samples was then quantified at a wavelength of 540 nm using a Multi-Mode Microplate Reader Synergy HTX spectrophotometer (Agilent Technologies, Santa Clara, CA, USA). Finally, the cell viability was calculated according to equation (4):

$$CV(\%) = \frac{OD_{sample} - OD_{blank}}{OD_{control} - OD_{blank}} \times 100 \quad (4)$$

where *CV(%)*: Cell viability; *OD*: Optical density of the wells containing cells with the evaluated sample (OD_{sample}), only cells ($OD_{control}$), and cell culture media without cells (OD_{blank}).

As per the producer's specifications, the positive control consists of untreated cells, MTT solution, and DMSO, while the negative control consists of only dead cells, MTT solution, and DMSO. The IC_{50} values denote the concentrations (75, 100, 125, 150, 175, and 200 µg/mL) at which both samples (*H. sphondylium* and HS-Ag system) displayed 50% cell viability for NHDF and HeLa cell lines. The cell viability data was plotted on a graph, and the IC_{50} values were subsequently calculated [92].

4.13. Statistical Analysis

All experiments were performed in triplicate for all samples, all calibration curves, and concentrations. Statistical analysis was carried out using Student's *t*-test and expressed as mean ± standard deviation (SD), using Microsoft Office Excel 2019 (Microsoft Corporation, Redmond, WA, USA). Dunnett's multiple comparison *post hoc* test following a one-way analysis of variance test (ANOVA) was used to analyze the results. *P*-values <0.05 were considered statistically significant.

 doi:10.20944/preprints202408.1706.v1

5. Conclusions

The study discusses the development of a novel plant-based system using AgNPs. FTIR, SEM, XRD, and DLS findings confirmed the successful incorporation of AgNPs into herbal matrix (*H. sphondylium*) particles and pores, resulting in the preparation of the HS-Ag system. Additionally, the antioxidant screening, antimicrobial, and *in vitro* cell viability investigations demonstrated that this innovative system exhibits enhanced biological properties compared to *H. sphondylium*. Collectively, this research work suggests that this new phytocarrier (HS-Ag system) holds promise for a wide range of medical applications.

Author Contributions: Conceptualization, A.E.S., L.E.B. and C.B.; methodology, A.E.S., G.B. and C.B.; validation, A.E.S., L.E.B. and C.B.; investigation, A.E.S., G.V., T.V., G.B., M.V.C. and C.B.; resources, A.E.S.; writing—original draft preparation, A.E.S., L.E.B., and G.D.M.; writing—review and editing, A.E.S., L.E.B., and G.D.M.; supervision, A.E.S., L.E.B., and C.B. All authors have read and agreed to the published version of the manuscript.

Funding: This work was supported by a grant from the European Research Executive Agency, Topic: HORIZON-MSCA-2022-SE-01-01, Type of action: HORIZON TMA MSCA Staff Exchanges, Project: 101131420—Exploiting the multifunctional properties of polyphenols: from wastes to high value products, Acronym: PHENOCYCLES.

Institutional Review Board Statement: Not applicable.

Informed Consent Statement: Not applicable.

Data Availability Statement: The original data presented in the study are openly available in [GoFile repository] at [https://gofile.me/7rkqY/KHgZHOglD].

Conflicts of Interest: The authors declare no conflicts of interest.

References

1. Bahadori, M.B.; Dinparast, L.; Zengin, G. The genus *Heracleum*: A comprehensive review on its phytochemistry, pharmacology, and ethnobotanical values as a useful herb. *Compr. Rev. Food Sci. Food Saf.* **2016**, *15*, 1018–1039. [https://doi.org/10.1111/1541-4337.12222] [https://pubmed.ncbi.nlm.nih.gov/33401836/]
2. Matarrese, E.; Renna, M. Prospects of hogweed (*Heracleum sphondylium* L.) as a new horticultural crop for food and non-food uses: A review. *Horticulturae* **2023**, *9*, 246. [https://doi.org/10.3390/horticulturae9020246]
3. Hosseinzadeh, Z.; Ramazani, A.; Razzaghi-Asl, N. Plants of the genus *Heracleum* as a source of coumarin and furanocoumarin. *J. Chem. Rev.* **2019**, *1*, 78–98. [https://doi.org/10.33945/SAMI/JCR.2019.1.7898]
4. Săvulescu T (Ed). *Flora R.P.R.*, 1st ed.; Romanian Academy Publishing House: Bucharest, Romania, 1958; Volume VI, pp. 326–334, 621–633 (in Romanian).
5. Tutin, T.G.; Heywood, V.H.; Burges, N.A.; Moore, D.M.; Valentine, D.H.; Walters, S.M.; Webb, D.A. (Eds). *Flora Europaea. Vol. 2: Rosaceae to Umbelliferae*, 1st ed.; Cambridge University Press: Cambridge, UK, 1968, pp. 315–319, 364–366.
6. Ciocârlan, V. *Flora ilustrată a României. Pteridophyta et Spermatophyta*, 3rd ed.; Ceres Publishing House: Bucharest, Romania, 2009; pp. 461–466, 496–498 (in Romanian).
7. Sârbu, I.; Ştefan, N.; Oprea A. *Plante vasculare din România. Determinator ilustrat de teren*. 1st ed.; Victor B Victor Publishing House: Bucharest, Romania, 2013; pp. 404–416, 444–446 (in Romanian).
8. Benedec, D.; Hanganu, D.; Filip, L.; Oniga, I.; Tiperciuc, B.; Olah, N.K.; Gheldiu, A.M.; Raita, O.; Vlase, L. Chemical, antioxidant and antibacterial studies of Romanian *Heracleum sphondylium*. *Farmacia* **2017**, *65*, 252–256. [https://farmaciajournal.com/wp-content/uploads/2017-02-art-15-Benedec_Oniga_Vlase_252-256.pdf]
9. İşcan, G.; Demirci, F.; Kürkçüoğlu, M.; Kıvanç, M.; Başer, K.H.C. The bioactive essential oil of *Heracleum sphondylium* L. subsp. *ternatum* (Velen.) Brummitt. *Z. Naturforsch. C J. Biosci.* **2003**, *58*, 195–200. [https://doi.org/10.1515/znc-2003-3-410] [https://pubmed.ncbi.nlm.nih.gov/12710728/]
10. Uysal, A.; Ozer, O.Y.; Zengin, G.; Stefanucci, A.; Mollica, A.; Picot-Allain, C.M.N.; Mahomoodally, M.F. Multifunctional approaches to provide potential pharmacophores for the pharmacy shelf: *Heracleum sphondylium* L. subsp. *ternatum* (Velen.) Brummitt. *Comput. Biol. Chem.* **2019**, *78*, 64-73. [https://doi.org/10.1016/j.compbiolchem.2018.11.018] [https://pubmed.ncbi.nlm.nih.gov/30500554/]
11. Ozek, T.; Demirci, B.; Baser, K.H.C. Comparative study of the essential oils of *Heracleum sphondylium* ssp. *ternatum* obtained by micro- and hydro-distillation methods. *Chem. Nat. Compd.* **2002**, *38*, 48–50. [https://doi.org/10.1023/A:1015777614626]

12. Senejoux, F.; Demougeot, C.; Cuciureanu, M.; Miron, A.; Cuciureanu, R.; Berthelot, A.; Girard-Thernier, C. Vasorelaxant effects and mechanisms of action of *Heracleum sphondylium* L. (*Apiaceae*) in rat thoracic aorta. *J. Ethnopharmacol.* **2013**, *147*, 536–539. [https://doi.org/10.1016/j.jep.2013.03.030] [https://pubmed.ncbi.nlm.nih.gov/23541934/]
13. Ergene, A.; Guler, P.; Tan, S.; Mirici, S.; Hamzaoglu, E.; Duran, A. Antibacterial and antifungal activity of *Heracleum sphondylium* subsp. *artvinense*. *Afr. J. Biotechnol.* **2006**, *5*, 1087–1089. [https://academicjournals.org/journal/AJB/article-full-text-pdf/4597B636392]
14. Maggi, F.; Quassinti, L.; Bramucci, M.; Lupidi, G.; Petrelli, D.; Vitali, L.A.; Papa, F.; Vittori, S. Composition and biological activities of hogweed [*Heracleum sphondylium* L. subsp. *ternatum* (Velen.) Brummitt] essential oil and its main components octyl acetate and octyl butyrate. *Nat. Prod. Res.* **2014**, *28*, 1354–1363. [https://doi.org/10.1080/14786419.2014.904311] [https://pubmed.ncbi.nlm.nih.gov/24697288/]
15. Ušjak, L.; Sofrenić, I.; Tešević, V.; Drobac, M.; Niketić, M.; Petrović, S. Fatty acids, sterols, and triterpenes of the fruits of 8 *Heracleum* taxa. *Nat. Prod. Commun.* **2019**, *14*, 1–7. [https://doi.org/10.1177/1934578X19856788]
16. Fierascu, R.C.; Padure, I.M.; Avramescu, S.M.; Ungureanu, C.; Bunghez, R.I.; Ortan, A.; Dinu-Pirvu, C.; Fierascu, I.; Soare, L.C. Preliminary assessment of the antioxidant, antifungal and germination inhibitory potential of *Heracleum sphondylium* L. (*Apiaceae*). *Farmacia* **2016**, 64, 403–408. [https://farmaciajournal.com/wp-content/uploads/2016-03-art-13-Fierascu_403-408.pdf]
17. Matejic, J.S.; Dzamic, A.M.; Mihajilov-Krstev, T.; Ristic, M.S.; Randelovic, V.N.; Krivošej, Z.Đ.; Marin, P.D. Chemical composition, antioxidant and antimicrobial properties of essential oil and extracts from *Heracleum sphondylium* L. *J. Essent. Oil Bear. Plants* **2016**, *19*, 944–953. [https://doi.org/10.1080/0972060X.2014.986538]
18. Yang, L.; Wen, K.-S.; Ruan, X.; Zhao, Y.-X.; Wei, F.; Wang, Q. Response of plant secondary metabolites to environmental factors. *Molecules* **2018**, *23*, 762. [https://doi.org/10.3390/molecules23040762] [https://pubmed.ncbi.nlm.nih.gov/29584636/]
19. Segneanu, A.E.; Grozescu, I.; Sfirloaga, P. The influence of extraction process parameters of some biomaterials precursors from *Helianthus annuus*. *Dig. J. Nanomater. Biostruct.* **2013**, 8, 1423–1433. [https://chalcogen.ro/1423_Segneanu.pdf]
20. Popescu, C.; Fitigau, F.; Segneanu, A.E.; Balcu, I.; Martagiu, R.; Vaszilcsin, C.G. Separation and characterization of anthocyanins by analytical and electrochemical methods. *Environ. Eng. Manag. J.* **2011**, *10*, 697–701. [https://doi.org/10.30638/eemj.2011.093]
21. Vaszilcsin, C.G.; Segneanu, A.E.; Balcu, I.; Pop, R.; Fitigău, F.; Mirica, M.C. Eco-friendly extraction and separation methods of capsaicines. *Environ. Eng. Manag. J.* **2010**, *9*, 971–976. [https://doi.org/10.30638/eemj.2010.130]
22. Segneanu, A.E.; Damian, D.; Hulka, I.; Grozescu, I.; Salifoglou, A. A simple and rapid method for calixarene-based selective extraction of bioactive molecules from natural products. *Amino Acids* **2016**, *48*, 849–858. [https://doi.org/10.1007/s00726-015-2132-9] [https://pubmed.ncbi.nlm.nih.gov/26597796/]
23. Emran, T.B.; Shahriar, A.; Mahmud, A.R.; Rahman, T.; Abir, M.H.; Siddiquee, M.F.R.; Ahmed, H.; Rahman, N.; Nainu, F.; Wahyudin, E.; et al. Multidrug resistance in cancer: Understanding molecular mechanisms, immunoprevention and therapeutic approaches. *Front. Oncol.* **2022**, *12*, 891652. [https://doi.org/10.3389/fonc.2022.891652] [https://pubmed.ncbi.nlm.nih.gov/35814435/]
24. Nath, R.; Roy, R.; Barai, G.; Bairagi, S.; Manna, S.; Chakraborty, R. Modern developments of nano based drug delivery system by combined with phytochemicals – presenting new aspects. *Int. J. Sci. Res. Sci. Technol.* **2021**, *8*, 107–129. [https://doi.org/10.32628/IJSRST218422]
25. Aparicio-Blanco, J.; Vishwakarma, N.; Lehr, C.M.; Prestidge, C.A.; Thomas, N.; Roberts, R.J.; Thorn, C.R.; Melero, A. Antibiotic resistance and tolerance: What can drug delivery do against this global threat? *Drug Deliv. Transl. Res.* **2024**, *14*, 1725–1734. [https://doi.org/10.1007/s13346-023-01513-6] [https://pubmed.ncbi.nlm.nih.gov/38341386/]
26. Ahmed, S.K.; Hussein, S.; Qurbani, K.; Ibrahim, R.H.; Fareeq, A.; Mahmood, K.A.; Mohamed, M.G. Antimicrobial resistance: Impacts, challenges, and future prospects. *J. Med. Surg. Publ. Health* **2024**, *2*, 100081. [https://doi.org/10.1016/j.glmedi.2024.100081]
27. Patra, J.K.; Das, G.; Fraceto, L.F.; Campos, E.V.R.; del Pilar Rodriguez-Torres, M.; Acosta-Torres, L.S.; Diaz-Torres, L.A.; Grillo, R.; Swamy, M.K.; Sharma, S.; et al. Nano based drug delivery systems: Recent developments and future prospects. *J. Nanobiotechnol.* **2018**, *16*, 71. [https://doi.org/10.1186/s12951-018-0392-8]
28. Sharma, S.; Chauhan, A.; Ranjan, A.; Mathkor, D.M.; Haque, S.; Ramniwas, S.; Tuli, H.S.; Jindal, T.; Yadav, V. Emerging challenges in antimicrobial resistance: Implications for pathogenic microorganisms, novel antibiotics, and their impact on sustainability. *Front. Microbiol.* **2024**, *15*, 1403168. [https://doi.org/10.3389/fmicb.2024.1403168] [https://pubmed.ncbi.nlm.nih.gov/38741745/]

29. Dewi, M.K.; Chaerunisaa, A.Y.; Muhaimin, M.; Joni, I.M. Improved activity of herbal medicines through nanotechnology. *Nanomaterials* **2022**, *12*, 4073. [https://doi.org/10.3390/nano12224073] [https://pubmed.ncbi.nlm.nih.gov/36432358/]
30. Malik, A.; Khan, J.M.; Alhomida, A.S.; Ola, M.S.; Alshehri, M.A.; Ahmad, A. Metal nanoparticles: Biomedical applications and their molecular mechanisms of toxicity. *Chem. Pap.* **2022**, *76*, 6073–6095. [https://doi.org/10.1007/s11696-022-02351-5]
31. Meher, A.; Tandi, A.; Moharana, S.; Chakroborty, S.; Mohapatra, S.S.; Mondal, A.; Dey, S.; Chandra, P. Silver nanoparticle for biomedical applications: A review. *Hybrid Adv.* **2024**, *6*, 100184. [https://doi.org/10.1016/j.hybadv.2024.100184]
32. Segneanu, A.-E.; Vlase, G.; Lukinich-Gruia, A.T.; Herea, D.-D.; Grozescu, I. Untargeted metabolomic approach of *Curcuma longa* to neurodegenerative phytocarrier system based on silver nanoparticles. *Antioxidants (Basel)* **2022**, *11*, 2261. [https://doi.org/10.3390/antiox11112261] [https://pubmed.ncbi.nlm.nih.gov/36421447/]
33. Činčala, Ľ.; Illeová, V.; Antošová, M.; Štefuca, V.; Polakovič, M. Investigation of plant sources of hydroperoxide lyase for 2(E)-hexenal production. *Acta Chim. Slovaca* **2015**, *8*, 156–165. [https://doi.org/10.1515/acs-2015-0027]
34. Milovanović, I.L.J.; Mišan, A.Č.; Sakač, M.B.; Čabarkapa, I.S.; Šarić, B.M.; Matić, J.J.; Jovanov, P.T. Evaluation of a GC-MS method for the analysis of oregano essential oil composition. *Food Feed Res.* **2009**, *36*, 75–79. [http://foodandfeed.fins.uns.ac.rs/uploads/Magazines/magazine_49/evaluation-of-a-gc-ms-method-for-the-analysis-of-oregano-essential-oil-composition.pdf]
35. Chen, Q.; Hu, X.; Li, J.; Liu, P.; Yang, Y.; Ni, Y. Preparative isolation and purification of cuminaldehyde and *p*-menta-1,4-dien-7-al from the essential oil of *Cuminum cyminum* L. by high-speed counter-current chromatography. *Anal. Chim. Acta.* **2011**, *689*, 149–154. [https://doi.org/10.1016/j.aca.2011.01.038] [https://pubmed.ncbi.nlm.nih.gov/21338771/]
36. Segneanu, A.-E.; Vlase, G.; Vlase, T.; Ciocalteu, M.-V.; Bejenaru, C.; Buema, G.; Bejenaru, L.E.; Boia, E.R.; Dumitru, A.; Boia, S. Romanian wild-growing *Chelidonium majus*—An emerging approach to a potential antimicrobial engineering carrier system based on AuNPs: *In vitro* investigation and evaluation. *Plants (Basel)* **2024**, *13*, 734. [https://doi.org/10.3390/plants13050734] [https://pubmed.ncbi.nlm.nih.gov/38475580/]
37. Mickus, R.; Jančiukė, G.; Raškevičius, V.; Mikalayeva, V.; Matulytė, I.; Marksa, M.; Maciūnas, K.; Bernatonienė, J.; Skeberdis, V.A. The effect of nutmeg essential oil constituents on Novikoff hepatoma cell viability and communication through Cx43 gap junctions. *Biomed. Pharmacother.* **2021**, *135*, 111229. [https://doi.org/10.1016/j.biopha.2021.111229] [https://pubmed.ncbi.nlm.nih.gov/33444950/]
38. Aminkhah, M.; Asgarpanah, J. GC-MS analysis of the essential oil from *Artemisia aucheri* Boiss. fruits. *J. Chil. Chem. Soc.* **2017**, *62*, 3581–3582. [https://doi.org/10.4067/s0717-97072017000303581]
39. Wijit, N.; Prasitwattanaseree, S.; Mahatheeranont, S.; Wolschann, P.; Jiranusornkul, S.; Nimmanpipug, P. Estimation of retention time in GC/MS of volatile metabolites in fragrant rice using principle components of molecular descriptors. *Anal. Sci.* **2017**, *33*, 1211–1217. [https://doi.org/10.2116/analsci.33.1211] [https://pubmed.ncbi.nlm.nih.gov/29129857/]
40. Wangchuk, P.; Keller, P.A.; Pyne, S.G.; Taweechotipatr, M.; Kamchonwongpaisan, S. GC/GC-MS analysis, isolation and identification of bioactive essential oil components from the Bhutanese medicinal plant, *Pleurospermum amabile*. *Nat. Prod. Commun.* **2013**, *8*, 1305–1308. [https://doi.org/10.1177/1934578X1300800930] [https://pubmed.ncbi.nlm.nih.gov/24273872/]
41. Al-Rubaye, A.F.; Kadhim, M.J.; Hameed, I.H. Determination of bioactive chemical composition of methanolic leaves extract of *Sinapis arvensis* using GC-MS technique. *Int. J. Toxicol. Pharmacol. Res.* **2017**, *9*, 163–178. [https://doi.org/10.5281/zenodo.12730256]
42. Kumar, A.; Kumari, P.; Somasundaram, S.T. Gas chromatography-mass spectrum (GC-MS) analysis of bioactive components of the methanol extract of halophyte, *Sesuvium portulacastrum* L. *Int. J. Adv. Pharm. Biol. Chem.* **2014**, *3*, 766–772. [https://www.ijapbc.com/files/07-10-2015/39-3396RR.pdf]
43. Viet, T.D.; Xuan, T.D.; Anh, L.H. α-Amyrin and β-amyrin isolated from *Celastrus hindsii* leaves and their antioxidant, anti-xanthine oxidase, and anti-tyrosinase potentials. *Molecules* **2021**, *26*, 7248. [https://doi.org/10.3390/molecules26237248] [https://pubmed.ncbi.nlm.nih.gov/34885832/]
44. Bianchi, F.; Careri, M.; Mangia, A.; Musci, M. Retention indices in the analysis of food aroma volatile compounds in temperature-programmed gas chromatography: Database creation and evaluation of precision and robustness. *J. Sep. Sci.* **2007**, *30*, 563–572. [https://doi.org/10.1002/jssc.200600393] [https://pubmed.ncbi.nlm.nih.gov/17444225/]
45. Segneanu, A.-E.; Cepan, M.; Bobica, A.; Stanusoiu, I.; Dragomir, I.C.; Parau, A.; Grozescu, I. Chemical screening of metabolites profile from Romanian *Tuber* spp. *Plants (Basel)* **2021**, *10*, 540. [https://doi.org/10.3390/plants10030540] [https://pubmed.ncbi.nlm.nih.gov/33809254/]
46. Herrera-Calderon, O.; Chavez, H.; Enciso-Roca, E.C.; Común-Ventura, P.W.; Hañari-Quispe, R.D.; Figueroa-Salvador, L.; Loyola-Gonzales, E.L.; Pari-Olarte, J.B.; Aljarba, N.H.; Alkahtani, S.; et al. GC-MS profile, antioxidant activity, and *in silico* study of the essential oil from *Schinus molle* L. leaves in the

presence of mosquito juvenile hormone-binding protein (mJHBP) from *Aedes aegypti*. *Biomed. Res. Int.* **2022**, *2022*, 5601531. [https://doi.org/10.1155/2022/5601531] [https://pubmed.ncbi.nlm.nih.gov/35615009/]

47. Słowiński, K.; Grygierzec, B.; Synowiec, A.; Tabor, S.; Araniti, F. Preliminary study of control and biochemical characteristics of giant hogweed (*Heracleum sosnowskyi* Manden.) treated with microwaves. *Agronomy* **2022**, *12*, 1335. [https://doi.org/10.3390/agronomy12061335]
48. Bicchi, C.; D'Amato, A.; Frattini, C.; Cappelletti, E.M.; Caniato, R.; Filippini, R. Chemical diversity of the contents from the secretory structures of *Heracleum sphondylium* subsp. *sphondylium*. *Phytochemistry* **1990**, *29*, 1883–1887. [https://doi.org/10.1016/0031-9422(90)85033-C]
49. Majidi, Z.; Sadati Lamardi, S.N. Phytochemistry and biological activities of *Heracleum persicum*: A review. *J. Integr. Med.* **2018**, *16*, 223–235. [https://doi.org/10.1016/j.joim.2018.05.004] [https://pubmed.ncbi.nlm.nih.gov/29866612/]
50. Hazrati, S.; Mollaei, S.; Rabbi Angourani, H.; Hosseini, S.J.; Sedaghat, M.; Nicola, S. How do essential oil composition and phenolic acid profile of *Heracleum persicum* fluctuate at different phenological stages? *Food Sci. Nutr.* **2020**, *8*, 6192–6206. [https://doi.org/10.1002/fsn3.1916] [https://pubmed.ncbi.nlm.nih.gov/33282270/]
51. Wu, Z.; Zhong, A.; Shen, P.; Zhu, J.; Li, L.; Xia, G.; Zang, H. Chemical constituents, antioxidant and antibacterial activities of essential oil from the flowering aerial parts of *Heracleum moellendorffii* Hance. *Cogent Food Agric.* **2024**, *10*, 2325198. [https://doi.org/10.1080/23311932.2024.2325198]
52. Segneanu, A.-E.; Vlase, G.; Vlase, T.; Bita, A.; Bejenaru, C.; Buema, G.; Bejenaru, L.E.; Dumitru, A.; Boia, E.R. An innovative approach to a potential neuroprotective *Sideritis scardica*–clinoptilolite phyto-nanocarrier: *In vitro* investigation and evaluation. *Int. J. Mol. Sci.* **2024**, *25*, 1712. [https://doi.org/10.3390/ijms25031712] [https://pubmed.ncbi.nlm.nih.gov/38338989/]
53. Ahmed, B.A.; Mustafa, Y.F.; Ibrahim, B.Y. Isolation and characterization of furanocoumarins from golden delicious apple seeds. *J. Med. Chem. Sci.* **2022**, *5*, 537–545. [https://doi.org/10.26655/JMCHEMSCI.2022.4.9]
54. Ren, F.; Hu, J.; Dang, Y.; Deng, H.; Ren, J.; Cheng, S.; Tan, M.; Zhang, H.; He, X.; Yu, H.; et al. Sphondin efficiently blocks HBsAg production and cccDNA transcription through promoting HBx degradation. *J. Med. Virol.* **2023**, *95*, e28578. [https://doi.org/10.1002/jmv.28578] [https://pubmed.ncbi.nlm.nih.gov/36846971/]
55. Krysa, M.; Szymańska-Chargot, M.; Zdunek, A. FT–IR and FT–Raman fingerprints of flavonoids – A review. *Food Chem.* **2022**, *393*, 133430. [https://doi.org/10.1016/j.foodchem.2022.133430] [https://pubmed.ncbi.nlm.nih.gov/35696953/]
56. Bensemmane, N.; Bouzidi, N.; Daghbouche, Y.; Garrigues, S.; de la Guardia, M.; El Hattab, M. Quantification of phenolic acids by partial least squares Fourier-transform infrared (PLS–FTIR) in extracts of medicinal plants. *Phytochem. Anal.* **2021**, *32*, 206–221. [https://doi.org/10.1002/pca.2974] [https://pubmed.ncbi.nlm.nih.gov/32666562/]
57. Zając, A.; Michalski, J.; Ptak, M.; Dymińska, L.; Kucharska, A.Z.; Zierkiewicz, W.; Hanuza, J. Physicochemical characterization of the loganic acid – IR, Raman, UV–Vis and luminescence spectra analyzed in terms of quantum chemical DFT approach. *Molecules* **2021**, *26*, 7027. [https://doi.org/10.3390/molecules26227027] [https://pubmed.ncbi.nlm.nih.gov/34834118/]
58. Muhammad, A.; Idris, M.M.; Ali, U.; Umar, A.; Sirat, H.M. Characterization and tyrosinase activities of a mixture of β-sitosterol and stigmasterol from *Bauhinia rufescens* Lam. *Acta Pharm. Indones.* **2023**, *11*, 6284. [https://doi.org/10.20884/1.api.2023.11.2.6284]
59. Yadav, R.K.; Yadav, B.; Srivastav, G.; Jha, O.; Yadav, R.A. Conformational, structural and vibrational studies of estragole. *Vib. Spectrosc.* **2021**, *117*, 103317. [https://doi.org/10.1016/j.vibspec.2021.103317]
60. Danish, M.S.S.; Estrella-Pajulas, L.L.; Alemaida, I.M.; Grilli, M.L.; Mikhaylov, A.; Senjyu, T. Green synthesis of silver oxide nanoparticles for photocatalytic environmental remediation and biomedical applications. *Metals* **2022**, *12*, 769. [https://doi.org/10.3390/met12050769]
61. Galatage, S.T.; Hebalkar, A.S.; Dhobale, S.V.; Mali, O.R.; Kumbhar, P.S.; Nikade, S.V.; Killedar, S.G. Silver nanoparticles: Properties, synthesis, characterization, applications and future trends. In *Silver Micro-Nanoparticles—Properties, Synthesis, Characterization, and Applications*; Kumar, S., Kumar, P., Pathak, C.S., Eds.; IntechOpen: London, UK, 2021; Chapter 4. [https://doi.org/10.5772/intechopen.99173]
62. Vanaja, M.; Annadurai, G. *Coleus aromaticus* leaf extract mediated synthesis of silver nanoparticles and its bactericidal activity. *Appl. Nanosci.* **2013**, *3*, 217–223. [https://doi.org/10.1007/s13204-012-0121-9]
63. Rajasekhar Reddy, G.; Bertie Morais, A.; Nagendra Gandhi, N. 2,2-Diphenyl-1-picrylhydrazyl free radical scavenging assay and bacterial toxicity of protein capped silver nanoparticles for antioxidant and antibacterial applications. *Asian J. Chem.* **2013**, *25*, 9249–9254. [https://doi.org/10.14233/ajchem.2013.15215]
64. Segneanu, A.-E.; Vlase, G.; Vlase, T.; Sicoe, C.A.; Ciocalteu, M.V.; Herea, D.D.; Ghirlea, O.-F.; Grozescu, I.; Nanescu, V. Wild-grown Romanian *Helleborus purpurascens* approach to novel chitosan phyto-nanocarriers—metabolite profile and antioxidant properties. *Plants (Basel)* **2023**, *12*, 3479. [https://doi.org/10.3390/plants12193479] [https://pubmed.ncbi.nlm.nih.gov/37836219/]

65. Dash, D.K.; Tyagi, C.K.; Sahu, A.K.; Tripathi, V. Revisiting the medicinal value of terpenes and terpenoids. In *Revisiting Plant Biostimulants*; Meena, V.S., Parewa, H.P., Meena, S.K., Eds.; IntechOpen: London, UK, 2022; Chapter 5. [https://doi.org/10.5772/intechopen.102612]
66. Mahendra, C.K.; Tan, L.T.H.; Lee, W.L.; Yap, W.H.; Pusparajah, P.; Low, L.E.; Tang, S.Y.; Chan, K.G.; Lee, L.H.; Goh, B.H. Angelicin – A furocoumarin compound with vast biological potential. *Front. Pharmacol.* **2020**, *11*, 366. [https://doi.org/10.3389/fphar.2020.00366] [https://pubmed.ncbi.nlm.nih.gov/32372949/]
67. Liga, S.; Paul, C.; Péter, F. Flavonoids: Overview of biosynthesis, biological activity, and current extraction techniques. *Plants (Basel)* **2023**, *12*, 2732. [https://doi.org/10.3390/plants12142732] [https://pubmed.ncbi.nlm.nih.gov/37514347/]
68. Zhang, Y.; Cai, P.; Cheng, G.; Zhang, Y. A brief review of phenolic compounds identified from plants: Their extraction, analysis, and biological activity. *Nat. Prod. Commun.* **2022**, *17*, 1–14. [https://doi.org/10.1177/1934578X211069721]
69. Lobiuc, A.; Pavăl, N.-E.; Mangalagiu, I.I.; Gheorghiţă, R.; Teliban, G.-C.; Amăriucăi-Mantu, D.; Stoleru, V. Future antimicrobials: Natural and functionalized phenolics. *Molecules* **2023**, *28*, 1114. [https://doi.org/10.3390/molecules28031114] [https://pubmed.ncbi.nlm.nih.gov/36770780/]
70. Yang, J.; Dai, X.; Xu, H.; Tang, Q.; Bi, F. Regulation of ferroptosis by amino acid metabolism in cancer. *Int. J. Biol. Sci.* 2022, *18*, 1695–1705. [https://doi.org/10.7150/ijbs.64982] [https://pubmed.ncbi.nlm.nih.gov/35280684/]
71. Holeček, M. Aspartic acid in health and disease. *Nutrients* **2023**, *15*, 4023. [https://doi.org/10.3390/nu15184023] [https://pubmed.ncbi.nlm.nih.gov/37764806/]
72. Coniglio, S.; Shumskaya, M.; Vassiliou, E. Unsaturated fatty acids and their immunomodulatory properties. *Biology* **2023**, *12*, 279. [https://doi.org/10.3390/biology12020279] [https://pubmed.ncbi.nlm.nih.gov/36829556/]
73. Vezza, T.; Canet, F.; de Marañón, A.M.; Bañuls, C.; Rocha, M.; Víctor, V.M. Phytosterols: Nutritional health players in the management of obesity and its related disorders. *Antioxidants (Basel)* **2020**, *9*, 1266. [https://doi.org/10.3390/antiox9121266] [https://pubmed.ncbi.nlm.nih.gov/33322742/]
74. Mahendra, M.Y.; Purba, R.A., Dadi, T.B., Pertiwi, H. Estragole: A review of its pharmacology, effect on animal health and performance, toxicology, and market regulatory issues. *Iraqi J. Vet. Sci.* **2023**, *37*, 537–546. [https://doi.org/10.33899/ijvs.2022.135092.2445]
75. Szczepaniak, O.; Cielecka-Piontek, J.; Kobus-Cisowska, J. Hypoglycaemic, antioxidative and phytochemical evaluation of *Cornus mas* varieties. *Eur. Food Res. Technol.* **2021**, *247*, 183–191. [https://doi.org/10.1007/s00217-020-03616-7]
76. Ambwani, S.; Tandon, R.; Ambwani, T.K. Metal nanodelivery systems for improved efficacy of herbal drugs. *Biosci. Biotechnol. Res. Asia* **2019**, *16*, 251–261. [https://doi.org/10.13005/bbra/2741]
77. Bedlovičová, Z.; Strapáč, I.; Baláž, M.; Salayová, A. A brief overview on antioxidant activity determination of silver nanoparticles. *Molecules* **2020**, *25*, 3191. [https://doi.org/10.3390/molecules25143191] [https://pubmed.ncbi.nlm.nih.gov/32668682/]
78. Rehman, H.; Ali, W.; Ali, M.; Khan, N.Z.; Aasim, M.; Khan, A.A.; Khan, T.; Ali, M.; Ali, A.; Ayaz, M.; et al. *Delpinium uncinatum* mediated green synthesis of AgNPs and its antioxidant, enzyme inhibitory, cytotoxic and antimicrobial potentials. *PLoS One* **2023**, *18*, e0280553. [https://doi.org/10.1371/journal.pone.0280553] [https://pubmed.ncbi.nlm.nih.gov/37014921/]
79. Adil, M.; Filimban, F.Z.; Ambrin; Quddoos, A.; Sher, A.A.; Naseer, M. Phytochemical screening, HPLC analysis, antimicrobial and antioxidant effect of *Euphorbia parviflora* L. (*Euphorbiaceae* Juss.). *Sci. Rep.* **2024**, *14*, 5627. [https://doi.org/10.1038/s41598-024-55905-w] [https://pubmed.ncbi.nlm.nih.gov/38454096/]
80. Seneme, E.F.; dos Santos, D.C.; Silva, E.M.R.; Franco, Y.E.M.; Longato, G.B. Pharmacological and therapeutic potential of myristicin: A literature review. *Molecules* **2021**, *26*, 5914. [https://doi.org/10.3390/molecules26195914] [https://pubmed.ncbi.nlm.nih.gov/34641457/]
81. Kubo, I.; Fujita, K.; Nihei, K. Antimicrobial activity of anethole and related compounds from aniseed. *J. Sci. Food Agric.* **2008**, *88*, 242–247. [https://doi.org/10.1002/jsfa.3079]
82. Mahizan, N.A.; Yang, S.-K.; Moo, C.-L.; Song, A.A.-L.; Chong, C.-M.; Chong, C.-W.; Abushelaibi, A.; Lim, S.-H.E.; Lai, K.-S. Terpene derivatives as a potential agent against antimicrobial resistance (AMR) pathogens. *Molecules* **2019**, *24*, 2631. [https://doi.org/10.3390/molecules24142631] [https://pubmed.ncbi.nlm.nih.gov/31330955/]
83. Yang, W.; Chen, X.; Li, Y.; Guo, S.; Wang, Z.; Yu, X. Advances in pharmacological activities of terpenoids. *Nat. Prod. Commun.* **2020**, *15*, 1–13. [https://doi.org/10.1177/1934578X20903555]
84. Wasihun, Y.; Alekaw Habteweld, H.; Dires Ayenew, K. Antibacterial activity and phytochemical components of leaf extract of *Calpurnia aurea*. *Sci. Rep.* **2023**, *13*, 9767. [https://doi.org/10.1038/s41598-023-36837-3] [https://pubmed.ncbi.nlm.nih.gov/37328478/]
85. Nga, N.T.H.; Ngoc, T.T.B.; Trinh, N.T.M.; Thuoc, T.L.; Thao, D.T.P. Optimization and application of MTT assay in determining density of suspension cells. *Anal. Biochem.* **2020**, *610*, 113937. [https://doi.org/10.1016/j.ab.2020.113937] [https://pubmed.ncbi.nlm.nih.gov/32896515/]

 doi:10.20944/preprints202408.1706.v1

86. Aslantürk, Ö.S. *In vitro* cytotoxicity and cell viability assays: Principles, advantages, and disadvantages. In *Genotoxicity—A Predictable Risk to Our Actual World*; Larramendy, M.L., Soloneski, S., Eds.; IntechOpen: London, UK, 2018; Chapter 1. [https://doi.org/10.5772/intechopen.71923]
87. Sirait, M.; Sinulingga, K.; Siregar, N.; Doloksaribu, M.E.; Amelia. Characterization of hydroxyapatite by cytotoxicity test and bending test. *J. Phys. Conf. Ser.* **2022**, *2193*, 012039. [[https://doi.org/10.1088/1742-6596/2193/1/012039]
88. Miura, N.; Shinohara, Y. Cytotoxic effect and apoptosis induction by silver nanoparticles in HeLa cells. *Biochem. Biophys. Res. Commun.* **2009**, *390*, 733–737. [https://doi.org/10.1016/j.bbrc.2009.10.039] [https://pubmed.ncbi.nlm.nih.gov/19836347/]
89. Kavaz, D.; Faraj, R.E. Investigation of composition, antioxidant, antimicrobial and cytotoxic characteristics from *Juniperus sabina* and *Ferula communis* extracts. *Sci. Rep.* **2023**, *13*, 7193. [https://doi.org/10.1038/s41598-023-34281-x] [https://pubmed.ncbi.nlm.nih.gov/37137993/]
90. Hossain, M.L.; Lim, L.Y.; Hammer, K.; Hettiarachchi, D.; Locher, C. A review of commonly used methodologies for assessing the antibacterial activity of honey and honey products. *Antibiotics (Basel)* **2022**, *11*, 975. [https://doi.org/10.3390/antibiotics11070975] [https://pubmed.ncbi.nlm.nih.gov/35884229/]
91. Andrews, J.M. Determination of minimum inhibitory concentrations. *J. Antimicrob. Chemother.* **2001**, *48(Suppl 1)*, 5–16. [https://doi.org/10.1093/jac/48.suppl_1.5] [https://pubmed.ncbi.nlm.nih.gov/11420333/]
92. Kar, S.; Sengupta, D.; Deb, M.; Shilpi, A.; Parbin, S.; Rath, S.K.; Pradhan, N.; Rakshit, M.; Patra, S.K. Expression profiling of DNA methylation-mediated epigenetic gene-silencing factors in breast cancer. *Clin. Epigenetics* **2014**, *6*, 20. [https://doi.org/10.1186/1868-7083-6-20] [https://pubmed.ncbi.nlm.nih.gov/25478034/]